HHS Public Access

Author manuscript

Dev Cell. Author manuscript; available in PMC 2023 November 21.

Published in final edited form as:

Dev Cell. 2022 November 21; 57(22): 2517–2532.e6. doi:10.1016/j.devcel.2022.10.007.

Endocardium-to-coronary artery differentiation during heart development and regeneration involves sequential roles of Bmp2 and Cxcl12/Cxcr4

Gaetano D'Amato[1], **Ragini Phansalkar**[1,2], **Jeffrey A. Naftaly**[1], **Xiaochen Fan**[1], **Zhainib A. Amir**[1], **Pamela E. Rios Coronado**[1], **Dale O. Cowley**[3], **Kelsey E. Quinn**[4], **Bikram Sharma**[5], **Kathleen M. Caron**[4], **Alessandra Vigilante**[6], **Kristy Red-Horse**[1,7,*]

[1.] Department of Biology, Stanford University, Stanford, USA

[2.] Department of Genetics, Stanford University School of Medicine, Stanford, USA

[3.] Animal Models Core, University of North Carolina, Chapel Hill, NC, USA

[4.] Department of Cell Biology and Physiology, University of North Carolina at Chapel Hill, Chapel Hill, USA

[5.] Department of Biology, Ball State University, Muncie, USA

[6.] Centre for Stem Cells and Regenerative Medicine & Institute for Liver Studies, King's College London, London, UK.

[7.] Institute for Stem Cell Biology and Regenerative Medicine, Stanford University School of Medicine, Stanford, CA, USA

SUMMARY

Endocardial cells lining the heart lumen are coronary vessel progenitors during embryogenesis. Reigniting this developmental process in adults could regenerate blood vessels lost during cardiac injury, but this requires additional knowledge on molecular mechanisms. Here, we use mouse genetics and scRNAseq to identify regulators of endocardial angiogenesis and precisely assess the role of CXCL12/CXCR4 signaling. Time-specific lineage tracing demonstrated that endocardial cells differentiated in coronary endothelial cells primarily at mid-gestation. A new mouse line reporting CXCR4 activity—along with cell-specific gene deletions—demonstrated it was specifically required for artery morphogenesis rather than angiogenesis. Integrating scRNAseq data of endocardial-derived coronary vessels from mid- and late-gestation identified a

[*]Lead Contact: kredhors@stanford.edu.

Contributions

G. D and K.R-H conceptualized study and wrote article. G.D., R.P., J.A.N., X. F., and Z. A. A. performed experiments. G.D. and A.V performed computational analysis. G.D., K.R-H., K.E.Q., and K.M.C. designed *Cxcr4-Tango* and provided experimental resources. D.O.C advised on and generated *Cxcr4-Tango.* B.S. provided experimental and manuscript. P.E.R.C. assisted with the neonatal injured. All authors reviewed the manuscript.

Declaration of Interests

None of the authors have competing financial interests to declare.

Bmp2-expressing transitioning population specific to mid-gestation. Bmp2 stimulated endocardial angiogenesis in vitro and in injured neonatal mouse hearts. Our data demonstrate how understanding the molecular mechanisms underlying endocardial angiogenesis can identify new potential therapeutic targets promoting revascularization of the injured heart.

eTOC blurd:

Identifying how coronary blood vessels develop from their progenitors could inspire therapies promoting revascularization of diseased hearts deprived of blood flow. D'Amato et al. show that Bmp2 stimulates coronary vessel development from endocardial cells in embryonic hearts and forced Bmp2 expression after birth reactivates endocardial-derived vascularization in injured neonatal hearts.

Graphical Abstract

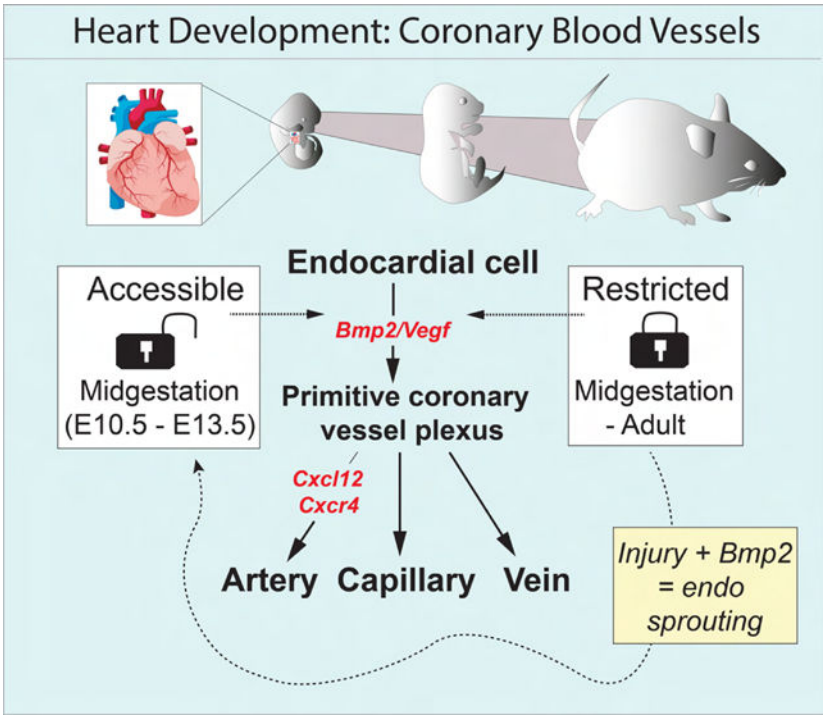

INTRODUCTION

Ischemic heart disease—the leading cause of death—commonly results from coronary artery occlusions and can lead to myocardial infarction (MI) and heart failure [1]. One therapeutic approach is to rebuild damaged coronary blood vessels. However, developing an intervention that regenerates coronary vasculature has proven difficult [2], likely due to our poor understanding of how cardiac blood vessels develop and respond to injury.

During development, most coronary vessel endothelial cells (CV ECs) arise from two spatially distinct cell types: endothelial cells (ECs) from the sinus venosus (SV), the venous inflow of heart, and endocardium (endo)[3–10]. The consensus is that sprouting angiogenesis

from SV and endo contribute to complementary regions of the vasculature [6–7,11,12], which are driven by different signaling pathways, epicardial VEGF-C/ELA versus intramyocardial VEGFA, respectively [4,5,8,13] The presence of dual progenitors for CV ECs has several benefits. It ensures fast vascularization of the growing heart [14] and provides alternative progenitors when angiogenesis from one source is abrogated [8].

Over the last decade, mouse genetics, lineage tracing, and single-cell RNA sequencing (scRNAseq) have been used to study how CV ECs sprout and migrate from the SV to form an immature vascular plexus that eventually differentiates into mature capillary, veins, and arteries [15–17] By comparison, there has been less focus on endo sprouting and major knowledge gaps remain.

Although molecular details are sparse, lineage tracing studies have progressively refined our understanding of when and where endo cells contribute to CV ECs in mice. Initially, *Nfatcl-Cre* lineage labeling showed the endo to be a major source of intramyocardial capillaries and arteries, while concomitant EC clonal analysis indicated most contribution occurred in and near the septum [3,4] Subsequently, a new *Cre* line allowing temporal control of lineage labeling reported minimal contribution within ventricular free walls before birth, producing mostly septal CV ECs at this stage [10] The same tool also showed that a second wave of endo-derived CV ECs begin to populate the inner half of the free walls shortly after birth [7] From histological analyses, the authors concluded that this wave of CV ECs arose from endo cells that become trapped during the process of neonatal trabecular compaction, although alternative interpretations existed since endo in these experiments were marked at embryonic day (E)8. Indeed, a recent study employing a lineage labeling time course identified that the second wave derives from endo cells that differentiated into CV ECs at some point prior to E16.5 [18].

This restriction to embryonic stages is consistent with studies showing that endo angiogenesis does not normally occur during cardiac injury, in neonate and adult hearts [18,19] However, Vegf-B or Vegfr2 overexpression can induce some after MI [20,21]. Re-activating endo angiogenesis in adults is an attractive therapeutic strategy, particularly since ischemic injuries frequently localize to subendocardial myocardium. To reach this goal, we must learn more about normal development. Current critical outstanding questions include: at which precise time points between E8 and 16.5 do endo cells differentiate into CV ECs and what are the molecular players.

Here, we used pulse-chase lineage tracing and scRNAseq to further define the endo angiogenic window and discover molecular regulators. We found the endo-to-CV ECs transition occurring largely between E10.5–13.5, initially producing septal CV ECs that subsequently migrate outward to form vessel plexuses outside the septum. Ligand-receptor expression patterns suggested this migration involved Cxcl12/Cxcr4, but mouse genetics and a new mouse line reporting active Cxcr4 showed this axis functions primarily in artery morphogenesis. We next contrasted scRNAseq datasets from mid- and late-gestation. *Bmp2* was upregulated in CV ECs transitioning from the endo, which was present only mid-gestation. Bmp2 potentiated Vegf-A-induced angiogenesis, and forced *Bmp2* expression in neonatal hearts stimulated endo angiogenesis after MI. Our data highlight how

spatiotemporally restricted signaling influences the capability of endo cells to differentiate into CV ECs and that Bmp2 can re-activate this activity within favorable angiogenic/hypoxic environments.

RESULTS

Differentiation of endo to CV ECs is largely restricted to early heart development

Endo cells are known to produce CV ECs that first appear during mid-gestation embryogenesis through angiogenic sprouting and continue to increase in number during postnatal life. One unanswered question is at what stages during embryogenesis does cell fate conversion occur. To address this question, we sought to perform a time course of endo labeling to determine the exact window of time at which CV ECs are lineage traced from endo progenitors.

First, we needed to obtain and characterize a Tamoxifen-inducible *Cre* line that was specific for endo cells. We found that *BmxCreERT2;Rosa26*^{tdTomato} [22] mice very specifically labeled endo and arterial cells when given Tamoxifen on E8.5 (Suppl. Fig. 1A and D). Arterial labeling should not influence the following experiments since previous studies have established that artery ECs are not CV progenitors [23]. Immunostaining of E11.5 lineage-labeled hearts dosed at E8.5 and 9.5 (Fig. 1A) in tissue sections and whole mount preparations with the pan-endothelial markers Erg and Vegfr2 showed recombination in greater than 90% of endo cells, but less than 3% of the SV (Fig. 1B-C; suppl. Fig. 1H). Across the timepoints, we noted that endo-derived CVs appeared first at E11.5 when they were exclusively in the septum (Fig. 1B' and C). We confirmed that tdTomato lineage-labeled ECs within the septum were CV ECs by fluorescent *in situ* hybridization (FISH) on consecutive heart sections at E11.5 for CV ECs *(Cldn5)* and endo *(Npr3)* markers. TdTomato+ ECs in the septum expressed *Cldn5* and were negative for *Npr3* (Fig 1 D). We also confirmed that *Cre* activity was specifically restricted to endo cells and not in septal CV ECs. The ESR antibody was used to detect CreERT2 expression (Suppl. Fig. 1E-G). ESR cells colocalized with tdTomato specifically in the ventricular endo but not in the septal CV ECs, indicating that endothelial tdTomato expressing cells observed in the septum derived from endo lineage. At E12.5 and E13.5, lineage-labeled CV ECs were mostly on the ventral myocardium where they appeared to progressively spread from the midline over time (Fig. 1E-top panel and suppl. Fig. 1I-top panel). Quantification showed that greater than 80% of ventral CV ECs were labeled while less than 5% of dorsal CV ECs were labeled (Fig. 1F and suppl. Fig. 1I and J). Collectively, these patterns are consistent with previous studies and confirm the line's utility in specifically labeling the endo lineage [15,16].

We next labeled the endo at various stages and quantified lineage traced cells during development to establish when endo cells differentiated into CV ECs (Fig. 1G). For embryonic analysis, labeling was observed in CV ECs on the ventral side of the heart in whole mount preparations at E15.5. Surprisingly, there was very little contribution when endo cells were labeled after E11.5 (Fig 1H and I). The most robust contribution occurred with E8.5 labeling (Fig 1H and I). This was not due to reduced endo labeling with the later injection. Endo recombination was comparable in E15.5 heart sections induced at E9.5 and E12.5 (suppl. Fig. 2A and B), while many more CV ECs were labeled with the early dose

(suppl. Fig. 2A and C). Thus, endo cells differentiated into CV ECs primarily during early heart development—mostly prior to E12.5.

To ascertain whether the "second wave" of coronary expansion into the inner wall of the myocardium also arises from CV ECs that differentiated from endo early in development, we followed labeling at either E10.5, E13.5, or E17.5 out to postnatal day (P)7 (Fig. 1J). With all dosing strategies, more than 80% of endo cells were labelled (Fig. 1K and L). The E10.5 dose labeled approximately 80% of septal and more than 40% of the ventricular CV ECs while the E13.5 dose labeled much fewer septal cells but a similar number of those in the ventricle (Fig. 1K and L). In contrast, the E17.5 dose resulted in very little labeling of CV ECs (Fig. 1K and L). Note that the isolated labeling of coronary arteries at E17.5 is likely due to the expression of *Bmx* in arterial endothelial cells (Fig. 1K).

Our findings indicated that endo differentiation is spatiotemporally patterned and occurred almost exclusively during development. Most septal CV ECs arise during ventricular septation ~between E8.5 and 10.5 and labeling dynamics suggest they are the precursors of ventral CV ECs. During later stages, shortly after E13.5, there is minimal cell fate conversion at the septum, but differentiation is still populating the inner myocardial wall/papillary muscle of the ventricles. Finally, levels of differentiation are very low, but still present (~2.5%), in the inner myocardial wall/papillary muscle after E17.5. These data are in contrast with a previous model indicating that a second wave of CV ECs derives from postnatal endo differentiation [7], but consistent with a recent report demonstrating that this cell fate transition occurs mostly prior to E16.5 [18].

Cxcl12/Cxcr4 deletion has a greater effect on artery formation than endo angiogenesis

The above data suggest that a prominent pathway from endo to CV ECs is a cell fate conversion at the septum followed by migration of septal CV ECs ventrally to populate the front of the heart. The signal(s) driving this specific migration event have not been described. Cxcl12 and Cxcr4 are good candidates since they stimulate CV ECs migration during Zebrafish coronary development. However, Cavallero *et al.* detected the opposite in mouse hearts, i.e. increased SV sprouting upon *Cxcl12* or *Cxcr4* knockout. [25]. We specifically investigated their role in early endo angiogenesis. We found that *Cxcr4* was expressed in endo-derived CV ECs at the junction between the septum and ventral myocardium, but not in the endo (Fig. 2A and suppl. Fig. 3A). Left ventricle cardiomyocytes expressed *Cxcl12* (Fig. 2B and Suppl. 3B). Thus, *Cxcr4* and *Cxcl12* are at the right time and place to drive migration of endo-derived CV ECs into ventral myocardium.

Mouse genetics were used to test this hypothesis. Deletion of *Cxcr4* from linage-labeled endo cells using *BmxCreERT2* and early Tamoxifen dosing (E9.5) specifically knocked out the receptor in the endo-derived CV ECs (suppl. Fig. 3C). Surprisingly, endo-derived Erg+ CV ECs still populated the ventral myocardium (Fig. 2C and D). In contrast, artery differentiation was severely stunted. There was a four-fold decrease in Jag1+ arterial ECs on the ventral side of the heart (Fig. 2E and F). Similar phenotypes were observed when *Cxcl12* was removed from cardiomyocytes (Fig. 2G-J). Timed tamoxifen dosing confirmed our above results that the majority of endo to CV ECs differentiation occurs early in heart development. Specifically, deleting *Cxcr4* at E13.5 had no effect on either migration or

artery formation (Fig. 2K-M). These data indicate that even though *Cxcr4* and *Cxcl12* are expressed where the vessels spread from the septum, migration is not dramatically affected by knocking down these genes. Instead, the primary defect is artery formation which is only seen when deletion in induced at E9.5.

These data suggested that observing the location of receptor activation might be a better predictor of Cxcr4 function than ligand-receptor expression patterns. But there was currently no available mouse line with this capability. We generated a new knock-in mouse line for this purpose by adapting elements of the TANGO system [26,27] CRISPR/Cas9 was used to insert, immediately after the *Cxcr4* stop codon, a bicistronic construct sequentially containing: 1) A tobacco etch virus (TEV) protease recognition site followed by a tetracycline transcriptional activator (tTA); 2) a P2A selfcleaving peptide sequence and 3) a mouse Beta-arrestin-2 fused to TEV protease (Fig. 3A). When this line is crossed with a tTA-activated nuclear GFP reporter (H2B-GFP)[28], ligand binding was designed to recruit B-arrestin-TEV, which cleaves the tTA, allowing it to move into the nucleus and stimulate H2B-GFP expression (Fig. 3A). Indeed, we observed H2B-GFP expression that was depleted with doxycycline (Dox) administration in multiple organs (suppl. Fig. 3D). To confirm that H2B-GFP expression specifically monitored Cxcr4 receptor activity and was not merely a surrogate of its expression, we immunostained *Cxcr4^{tango};H2B-GFP* heart sections with Cxcr4 and Vegfr2. Many Cxcr4-expressing CV ECs were negative for H2B-GFP, showing that Cxcr4 expression does not automatically induce TANGO activation (Fig. 3B). Most of H2B-GFP-positive cells colocalized with endothelial Cxcr4 CV ECs indicating Cxcr4 activity (Fig. 3B). H2B-GFP-positive cells lacking Cxcr4 were hematopoietic, which may result from the high stability of this reporter system and reflect activation in the bone marrow and subsequent receptor downregulation in the periphery. Thus, our genetic system performed as expected.

To characterize Cxcr4 activation in coronary vessels, *Cxcr4^{tango};H2B-GFP* hearts were immunostained with Vegfr2 and Erg. We observed many H2B-GFP-positive cells in lineage-labeled hearts, including valve mesenchyme (suppl. Fig. 3E). Only 10% of capillary plexus CV ECs expressed the Cxcr4 activation marker, including those on the ventral side lineage-labeled from the endo (Fig. 3C and D, suppl. Fig. 3F). Consistent with a specific role for Cxcr4 in artery development (see Fig. 2E and F), approximately 90% of artery ECs expressed H2B-GFP in both stages analyzed (3C and D, suppl. Fig.5D). Interestingly, perivascular cells, likely pericytes and smooth muscle cells were also positive (Fig. 3C and suppl. Fig. 3F). These data establish the validity of a new tool for probing Cxcr4 activation and highlights how activation reporters can be better predictors of loss-of-function phenotypes than ligand-receptor expression.

To further investigate the impact of Cxcr4 deletion on endo-derived CV ECs, we performed scRNA-seq analysis on E17.5 *BmxCreERT2;Rosa26^{tdTomato}* lineage-labeled hearts in which the *Cxcr4flox* allele was removed from endo cells at E9.5. FACS-sorted CD31+/tdTomato+ cells from *Cxcr4* heterozygous (*Cxcr4$^{fl/+}$*, control) and *Cxcr4* knock-out (*Cxcr4$^{fl/fl}$*, mutant) hearts were collected and processed using the 10X Genomics platform (Fig. 3E). After quality control and filtering, *Cxcr4$^{fl/+}$* and *Cxcr4$^{fl/fl}$* samples were integrated for downstream analysis. Initial unbiased clustering and uniform manifold approximation and projection

(UMAP) analysis on the integrated dataset identified 11 cell clusters, all of them expressing *tdTomato* and including CV EC *(Clnd5, Fabp4)* and endo *(Npr3; Cdh11)* clusters in addition to other endo-derived cells (suppl. Fig. 4A and B). The ratio of CV ECs to all other cell types was the same in both genotypes, supporting the above observation that *Cxcr4* deletion does not inhibit CV EC differentiation from endo cells or their movement onto the heart (Fig. 3F and suppl. 4C and D). Subsetting non-cycling CV ECs identified two capillary (Cap1; Cap2, Fig. 3G) and two coronary arteries clusters (Art1; Art2, Fig. 3G). Based on our previous study, gene expression indicated that Cap1 corresponded to CV ECs in the septum and Cap 2 those in the ventricle free walls [29] Similarly, Art1 and 2 represent small and large artery ECs, respectively [29,30]. *Cxcr4* was expressed in Art1, Art2, and Cap1 with a 4-fold downregulation in $Cxcr4^{f/fl}$ (Fig. 3H and I).

Despite the decrease in *Cxcr4* expression in mutants and the highly penetrant mutant phenotype, the percentage of cells in artery clusters was the same (Fig. 3J). This suggests Cxcr4 does not affect capillary and artery EC differentiation, but rather artery morphogenesis, which agrees with the prominent known role of Cxcl12 during cell migration. Extracting cluster defining genes (Fig. 3K) and comparing their expression levels did reveal differential gene expression (Fig. 3L). For example, there was a reduction in gene expression of larger artery markers *(Mpg; Bmx; Fbln2; Gja5)* and VegfA and hypoxia-related genes *(Igfbp3; Kcne3; Bmx,* Fig. 3L and suppl. Fig. 4E and F). We propose that pre-artery specification is independent of Cxcr4, but that Cxcl12 signals artery ECs to migrate together to build mature artery.

ScRNAseq reveals a *Bmp2*+ transitioning population during early coronary development

Since Cxcl12/Cxcr4 signaling was critical at a later than expected stage during endo angiogenesis, i.e. artery differentiation, we next sought to discover the pathways involved in earlier steps in the process. scRNASeq was performed on endo and CV ECs from E12 $BmxCreERT2;Rosa26^{tdTomato}$ -lineage labeled hearts, which is the stage shortly after the onset of endo differentiation. Cells were FACS-sorted into CD31+/tdTomato+ (endo and its derivatives) and CD31+/tdTomato- (SV and its derivatives) populations and processed using the 10X Genomics platform (Fig. 4A). After quality control and filtering (Suppl. Fig. 5A and B and Methods), a total of 10,878 cells were available for cell type characterization. UMAP analysis identified 11 cell clusters (Fig. 4B). Cell type identities were assigned using known gene expression. Six clusters expressed the endo markers *Cdh11*, *Npr3,* and *Adgrg6* and were mostly *tdTomato+* (Fig. 4C and D). Two clusters of CV ECs expressed the capillary markers *Cld5* and *Fabp4* (Fig. 4C and D). Only a small fraction of *tdTomato+* cells were found in the CV EC clusters at this stage, indicating that most were derived from the SV (Fig. 4C and D). We also detected two clusters of valve endothelial cells *(Twist1+;Tbx20+)* containing approximately the same number of *tdTomato* positive and negative cells (Fig. 4C and D). These cells and lineage identities are consistent with our previous data and the above lineage tracing, validating the dataset for further analysis.

We next subsetted the data to increase the resolution of our CV angiogenesis analyses. The endo clusters closest to CV ECs in the UMAP (E1 and E4), the SV cluster, and the CV clusters (CV1 and CV2) were subjected to trajectory analysis using Slingshot [31], which

infers cell state transitions. SV cells were predicted to transition into CV1 while endo cells transitioned first into CV2—the CV cluster also positive for the lineage marker—and then CV1 (Fig. 4E and Suppl. Fig. 5E). We next plotted the 50 most relevant genes reconstructing these cell state transitions (Suppl. Fig. 5F). Along the trajectory E4-E1-CV2, we observed a down-regulation of endo-defining genes *(Cdh11; Npr3; Irx5)* as the cells became CV ECs *(Cldn5; Fabp4).* This was accompanied by an induction of protein synthesis and metabolic related genes *(Ybx3; Eif5a; Aldoa)* (Fig. 4F and Suppl. Fig. 5F).

Differential gene expression (DEG) values comparing CV2 to aggregated E1, E4, and CV1 were calculated to search for genes that might have a specific role in endo angiogenesis. We found up-regulation of Vegf-A-induced genes (*Igfbp3*; *Esm1)* in CV2 (Fig. 4G), which is consistent with previous data demonstrating that endo sprouting involves Vegf-A while SV sprouting is instead stimulated by Vegf-C and Ela [4,11,12] During DEG analysis, *Bmp2* stood out as being particularly specific to CV2 (Fig. 4G and 4H). Bmp2 is an attractive candidate because it's known to dramatically affect endo fate during valvulogenesis [32] Overall, previous studies showed that Bmp2 induces endo ECs to transition into valve mesenchyme by stimulating the endothelial-mesenchymal transition (endMT)[33,34], and *in vivo Bmp2* overexpression inhibits endo genes, driving cells into a mesenchymal state [35,36]. We therefore performed additional analysis of Bmp ligand and receptor signaling pathway genes.

A ligand-receptor interaction analysis tool, CellChat, identified the *Bmp2* ligand as being specifically expressed in CV2 while its receptor subunit *Bmpr1a* was specifically in endo cells (Fig. 4I). The complementary receptor subunit, *Bmpr2,* (Bmps signal through heterotetramers of two receptor subunits) was in all clusters analyzed (Fig. 4I). The other Bmp ligand detected was *Bmp4,* which was highly specific to SV sprouts (Fig 4I). A Chord plot representing Bmp interactions predicted Bmp2 from CV2 and Bmp4 from SV signaling to a subset of endo ECs within E1 and E4 (Fig. 4J).

In total, our trajectory analysis using scRNAseq with lineage labeling information indicated that a cluster of newly formed CVs expressing *Bmp2* signals to the adjacent endo, possibly to promote endo-to-CV ECs differentiation and/or angiogenesis. This model was reinforced by the results obtained using CytoTRACE [37], a trajectory analysis tool that uses the number of genes expressed to assign differentiation state. Here, an endo-transition through CV1 and then CV2 was seen where the CV2 "bridge" to CV1 was enriched for Bmp2 (Suppl Fig. 5G-K).

Late gestation scRNAseq lacks a prominent transitioning population

Because staged lineage analysis showed minimal endo-to-CV EC differentiation after E17.5 (see Fig. 1J and K), we hypothesized that critical cell states and genes could be identified by comparing early and late scRNAseq datasets. E17.5 hearts were harvested and subjected to the same pipeline as above (Fig. 4A), resulting in high quality data from 13,454 cells (Suppl. 5C and D). Gene expression identified CV ECs, endo cells, and valve cells, which separated into a total of 8 clusters (Fig. 5A). The endo cluster was primarily *tdTomato+* while approximately half of capillaries and arteries expressed the lineage label (Fig. 5B) consistent with previous lineage analysis. Veins were mostly *tdTomato-,* which is expected

giving their localization to mostly SV-derived regions (Fig. 5B and C)[12]. The most diverse population in the dataset was CV ECs, which clustered into the following subpopulations: 4 *Cldn5+, Apln+* capillary clusters (Capl and Cap2= non cycling ECs and Cap2 - Cap3= cycling ECs), a *Gja5+,Cxcl12+* arterial cluster, and a *Vwf+* vein cluster (Fig. 5C). In contrast to the E12 dataset, there was no population bridging endo cells and CV ECs in the UMAP (compare Fig. 5A with Fig. 4B), a result also observed using CytoTRACE (Suppl. Fig. 6A-C). These data agreed with lineage tracing experiments (Fig. 1F-K and [18]), further indicating that most endo-to-CV EC fate transitions occur before E17.5.

Next, data from both time points were integrated to further explore the potential absence of a transitioning population at E17.5. After integration, 10 clusters were detected and annotated based on their nomenclature in the single datasets (Fig.5D and Suppl Fig. 6D). Endo cells across the two datasets mostly overlapped, suggesting that the endo cell state may not dramatically change over developmental time (Fig. 5D and E; Suppl Fig. 6E). Similarly, capillary clusters CV1 and Cap1 from E12 and E17.5, respectively, were also largely indistinguishable. In contrast, cells within CV2 from the E12 sample were clustered apart from the rest of E17.5 capillary clusters (Fig. 5D and E; Suppl Fig. 6F). The UMAP plot and trajectory analysis showed that CV2 cells were unique to E12, and that they existed in a transcriptional state between endo and CV1/Cap (Fig. 5D and E). These data further suggest that CV2 is an immature population of transitioning CV ECs only present at the earlier developmental stage.

Integrated data also confirmed that *Bmp2* was specific to E12 CV2 (the putative transition population), and the *Cxcl12/Cxcr4* axis specific to later artery populations (Fig. 5F and G). CellChat did not predict Bmp2 signaling from CV ECs to endo ECs at E17.5 as it did for E12 (Fig. 5H). However, Bmp4 was still predicted to be an autocrine signal within the vein compartment (Fig. 5H), which is consistent with previous studies demonstrating BMP as the vein specification factor early in development [13]. Interrogation of the Cxcl pathway predicted autocrine Cxcl12/Cxcr4 signaling within the arterial cluster. Interestingly, the Cxcl12 sink receptor *Cxcr7* was expressed in Endo, VE, and Vein clusters, suggesting a possible role for opposing arterial differentiation in veins (Fig. 5H and I). In total, in-silico-predicted ligand-receptor pairs support our findings that Cxcl12/Cxcr4 signaling in the developing heart is most critical for artery development, and that Bmp2 might be a signal stimulating the endo-to-CV EC transition, specifically at early stages.

Exogenous Bmp2 facilitates Vegf-A-induced endo angiogenesis

To test our hypothesis that Bmp2 induces early endo angiogenesis, we performed an *in vitro* coronary sprouting assay using lineage labeled E10.5 heart ventricle explants cultured on Matrigel for 6 days with different combinations of recombinant proteins (Fig. 6A). There was no sprouting of Vegfr2-positive vessels in wells containing either control vehicles or Bmp2 alone (Fig. 6B and C). At the 20ng/ml concentration, Vegf-A stimulated sprouting, but only 20% of vessels were tdTomato-positive, indicating that most did not derive from the endo (Fig. 6B and C). In contrast, explants treated with both Vegf-A and Bmp2 exhibited robust sprouting, most of which involved endo-derived ECs (Fig. 6B and C). These data demonstrated that, at least in this assay, Bmp2 alone does not induce CV EC outgrowth,

but it does greatly enhance Vegf-A-stimulated endo angiogenesis. Next, we decided to investigate whether inhibiting Bmp signaling impaired early endo-angiogenesis *in vivo*. Pregnant *BmxCreERT2;Rosa*^{tdTomato} females given Tamoxifen at E9.5 were treated with the BMP receptor antagonist LDN-193189. Then, angiogenesis was assessed in E12.5 embryonic hearts. LDN-193189 treatment caused a significant reduction of endo-derived CV ECs in the septal region of *BmxCreERT2;Rosa*^{tdTomato} hearts (Fig. 6 D and E) but no difference in the number of endo cells (Fig. 6 D and E). Surprisingly, there appeared to be a compensatory expansion of a non-endo-derived CV EC population, upon BMP receptor inhibition (Fig. 6D), which may be from the small endo lineage negative population of unknown identity in the septum (see Fig. 1C). Taken together, these data support our model that Bmp signaling facilitates endo angiogenesis.

We next investigated if Bmp2 could enhance endo angiogenesis in the context of injury. *BmxCreERT2;Rosa*^{tdTomato} neonates were injected with Tamoxifen and 2 days later subjected to MI through a permanent left coronary artery (LCA) ligation. To test the effect of locally delivered Bmp2, we generated an adeno-associated viral vectors expressing either Bmp2 (AAV-Bmp2) or GFP (control, AAV-GFP) under the control of the cardiac troponin T (cTnT) promoter. AVVs were administrated immediately after MI (Fig. 6F). One week post-MI, transduced hearts already showed widespread GFP expression in cardiomyocytes and qualitatively increased angiogenesis from the endo in Bmp2-treated samples (Suppl. Fig. 7). Quantification at two weeks post-MI, showed that AAV-Bmp2 hearts had more than a twofold increase in endo-derived CV ECs adjacent to the endo (Fig. 6G-H). Since Vegf-A is expected to be upregulated upon MI, the difference in AAV-Bmp2's effect in non-injured and MI is similar to explants where Vegf-A is required for Bmp2's activity. These data, coupled with the observation that Bmp2 is specific to a transitioning population, supports the model that Bmp2 is involved in stimulating early endocardial angiogenesis, potentially through new sprouts signaling to endo cells.

Discussion

Endo cells lining the heart chambers produce multiple cells in the heart, including CV ECs, mural cells, and valve mesenchyme [16]. Its intrinsic plasticity may offer a therapeutic approach for heart repair. Although the contribution of the endo-to-CVs has been studied and debated, the underlying molecular mechanisms and whether endo retains angiogenic potential throughout development remained largely unknown.

Our time resolved lineage tracing precisely defined when endo-derived CVs originate and how they populate the heart (Fig. 7A). Most differentiation occurs during septal development, producing septal CV ECs that migrate ventral and lateral into the intramyocardium. This pathway is supported by two observations: 1) few septal and ventral CVs are lineage traced when endo is labeled after E11.5 and 2) at this time point, the only endo-derived CVs are in the septum. A second event occurs later until E13.5 when endo cells differentiate and migrate laterally directly into the ventricular free walls. These data are supported by the absence of an apparent endo-to-CV transitioning population in our E17.5 scRNAseq data and the lack of phenotype when *Cxcr4* was deleted after E11.5. This is

consistent with recent findings that little, if any, endocardial differentiation occurs after birth [18].

Previous studies suggested that Cxcl12 is critical for coronary artery development primarily because of outflow tract expression where it attracts CV ECs to the aorta to initiate blood flow [25,38]. Deleting *Cxcl12* in either ventricular myocardium or the outflow tract provided supporting evidence because only the latter affected artery development. However, artery development was studied using tissue sectioning, which is most efficient at assessing the largest branches, while whole mount imaging could provide a more comprehensive assessment. The authors also did not consider endo versus SV. Thus, Cxcl12 in endo-derived CVs farther from the outflow tract and in smaller artery branches remained unexplored. Our data demonstrated that myocardial Cxcl12 is critical for endo- derived artery branches; scRNAseq identified a role in morphogenesis rather than artery EC differentiation (Fig. 7B).

Expression patterns and data in Zebrafish [24] suggested Cxcl12 might guide endo-derived sprouting angiogenesis. However, *Cxcr4* deletion did not dramatically affect the number of endo- derived CV ECs observed by immunofluorescence of scRNAseq. Instead, *Cxcr4* deletion specifically abrogated artery formation on the ventral side of the heart where endo-derived CVs are highly concentrated. These data underscored the importance of identifying the exact cells responding to a ligand within the tissue. Thus, we generated a new mouse model to monitor Cxcr4 activity at the single cell level using the TANGO system [26]. This tool showed that few ECs in the vascular plexus are activated whereas Cxcr4 activity is found in most artery ECs, supporting the genetic phenotypes and showing that only a subset *Cxcr4* expressing cells are activated by the ligand despite widespread *Cxcl12* expression (Fig. 7A). The ability to record Cxcr4 activity *in vivo* will be key to defining how secreted ligands find and activate receptors within the tissue during arterial development and regeneration.

Our demonstration that the endo's natural angiogenic potential is largely restricted to early development agrees with a recent study. indicating that the expansion of endo-derived CVs in the perinatal period is driven by angiogenesis of pre-existing CVs [18]. Therefore, these authors and our data provide evidence for an alternative interpretation of the previous model stating that *de novo* formation of postnatal CVs arise from endo differentiation occurring after birth [7]. An outstanding question is how/why do embryonic endo cells lose their angiogenic capacity? Integrating the E12 and E17.5 datasets showed that endo cells are transcriptionally similar across development, but that only E12 possess a "transitioning" population that specifically expresses *Bmp2.* These data suggest that stage specific Bmp2 could be involved in the restricted angiogenic period during development through a feed forward-like mechanism where new CV ECs signal to endo to stimulate more differentiation (Fig 7A).

Our *in vitro* and *in vivo* experiments supported the hypothesis that Bmp2 stimulates VegfA- dependent angiogenesis (Fig. 7C). Other studies observed that ectopic *Bmp2* expression throughout heart development induced uncontrolled EMT within the ventricular endocardium, resulting in a left ventricle non compaction (LVNC-like) phenotype [35]. In contrast, Bmp2 overexpression in neonatal hearts in our experiments did not produce

histologically obvious ventricular phenotypes, likely because of the short time window and much later stage. Parallels with the embryonic study do exist. There, overexpressed *Bmp2* caused endo cells to downregulate endo marker genes, which occurs when endo cells are differentiating into CV ECs [35,36].

Endo angiogenesis occurs in injured adult hearts overexpressing Vegf-B in cardiomyocytes [20] or Vegfr2 in endo cells [21], supporting the idea that adult endo cells do have the potential to differentiate. In total, our findings shed light on the molecular mechanisms orchestrating the cell fate conversion from endo-to-CVs and their role in arterial remodeling. We used this knowledge to promote the endo-to- CVs transition in injured neonatal hearts.

Limitations of the study

We provide an initial characterization on how Bmp2 signaling stimulates VegfA-dependent endocardial coronary genesis in developing hearts and how forced expression of Bmp2 reactivates the endo-to-CV EC transition in injured neonatal hearts. Future studies are required to determine whether Bmp2-depedent neovascularization of infarcted hearts is sufficient to ameliorates heart function and therefore be beneficial for heart regeneration. This will require a more detailed analysis on the effect of Bmp2 overexpression in adult mice subject to MI.

Star Methods

Resource availability

Lead Contact—Correspondence and requests for materials should be addressed to the Lead Contact, Kristy Red- Horse (kredhors@stanford.edu).

Materials Availability—*Cxcr4-Tango* transgenic mice were generated by the Animal Models Core Facility at the University North Carolina at Chapell Hill. Mice will be made available through requests to Drs. Red-Horse (kredhors@stanford.edu) and Caron (kathleencaron@med.unc.edu).

Data and code availability

- Gene count matrices from single-cell sequencing from E12 and E17.5 *BmxCreERT2;Rosa*^{tdTomato} hearts were generated in [29] and have been deposited on Dryad at: doi:https://doi.org/10.5061/dryad.h70rxwdjh. Custom code was generated using R to analyze the data and to generate plots. Single-cell RNA-seq data from E17.5 *BmxCreER T2;Rosa*^{tdTomato} ;Cxcr4$^{flox/+}$ and *BmxCreERT2;Rosa*^{tdTomato} ;Cxcr4$^{flox/+}$ have been deposited at GEO with the accession number: GSE214942 and are publicly available.
- This Paper does not report original code
- Any additional information required to reanalyze the data reported in this paper is available from the lead contact upon request.

Experimental model and subject detail

Mice—All mouse husbandry and experiments were performed in accordance with Stanford Institutional Animal Care and Use Committee (IACUC) guidelines. All mice were housed in a pathogen-free facility. A maximum of 5 adult mice were housed per cage. Animals were monitored daily for normal husbandry and any health concerns. Cages were kept under a 12-hour light and 12-hour dark cycle. Mouse lines used in this study were: wild type (CD1, Charles River Laboratories, Strain Code #022), *Cxcl12*$^{fl/fl}$ (The Jackson Laboratory, B6(FVB)-Cxcl12^{tm11Link}/J, Stock# 021773), *Cxcr4*^{fl,fl} (The Jackson Laboratory, B6.129P2-Cxcr4^{tm27zo}/J, Stock# 008767), *Rosa26*^{tdTomato} Cre reporter (The Jackson Laboratory, *B6.Cg-Gt(ROSA)26Sor*$^{tm9(CAG-TdTomato)Hze}$*/J,* Stock# 007909), *Rosa26*^{ntdTomato} Cre reporter (The Jackson Laboratory, B6.Cg-Gt(ROSA)26Sortm75.1$^{(CAG-tdTomato*)Hze}$/J, Stock# 025106), *Cxcl12-DsRed* (The Jackson Laboratory, *Cxcl12*^{tm21Sjm}*/J,* Stock# 022458), *pTRE-H2BGFP* (The Jackson *Tg*$^{(tetO-mSTm2RJ/GFP)47Efu}$/J, Stock# 005104), *BmxCreERT2* [22] All mice in this study were maintained on a mixed background.

Generation of a Cxcr4 Tango Knock-in allele—For the generation of Cxcr4-Tango we inserted Tango elements into the Cxcr4 endogenous locus by CRISPR/Cas9-mediated genome editing in C57BL/6J strain. Briefly: three guide RNAs overlapping the *Cxcr4* stop codon were selected for activity testing. Functional testing was performed by transfecting a mouse embryonic fibroblast cell line (MEF) with guide RNA and HiFiCas9 protein (Integrated DNA Technologies). Following transfection, the guide RNA target site was PCR amplified from transfected cells and analyzed by ICE (Synthego) to detect Cas9-mediated mutations. The guide RNA selected for genome editing in embryos was Cxcr4-g55B (protospacer sequence 5'- GTCTTTGCATAAGTGTTAGC-3'). 910 bp 5' and 1014 bp 3' homology arms were cloned into a plasmid donor vector flanking the Tango elements: 1) a codon-optimized tTA with preceding TEV protease cleavage site; 2) a P2A "self-cleaving" peptide sequence; 3) a Beta-arrestin-2-TEV protease fusion protein; 4) 3X stop codons, FRT site, and loxP-flanked SV40 late polyadenylation sequences. C57BL/6J zygotes were microinjected with 800 nM HiFiCas9 protein, 50 ng/ul guide RNA and 20 ng/ul supercoiled donor vector plasmid. Injected embryos were implanted in recipient pseudopregnant females. Eight resulting pups were screened by PCR for the presence of the knock- in allele. Two of 8 pups were positive for the knock-in event with primers spanning from outside of the homology arms to unique sequences in the knock-in allele. Both founders also showed evidence of vector backbone integration, consistent with the presence of a tandem integration event at the Cxcr4 target site. Founder animals were mated to C57BL/6J-Rosa26-CAG-Flpo transgenic animals to collapse tandem integration events to single-copy knock-ins. F1 animals heterozygous for the correct knock-in event and absence of vector backbone sequence were used for subsequent breeding to establish the knock-in colony. To genotype the *Cxcr4*-Tango knock-in allele we generated the following primers: P2A-SqF1_TGGAGACGTGGAGGAGAACC and Barr2- SqR1_GATGAT AAGC C GCACAGAGT.

Breeding, tamoxifen administration and doxycycline treatment—Timed pregnancies were determined by the morning day on which vaginal plug was found as E0.5. To activate inducible Cre, 4mg of 20mg/ml Tamoxifen (Sigma-Aldrich, T5648) was

administered to pregnant dams by oral gavage at E8.5 and E9.5. Two consecutive Tamoxifen doses were used to characterize the recombination rate of *BmxCreER* mouse line and for scRNAseq experiments. For time-course lineage tracing analysis and loss of function (LOF) experiments one dose of 4mg of Tamoxifen or 2mg of 4-OH tamoxifen (Sigma-Aldrich, H6278) was administrated at defined embryonic stage. For neonatal studies, two consecutive doses of 4mg Tamoxifen were administrated by oral gavage to nursing mom. In order to test the ability of doxycycline to effectively abolish H2B transcription mice were given food containing 200 mg of doxycycline per kg of diet (Bio-serv # S3888). Mice were given doxycycline containing food for six days prior to sacrifice and harvest of organs.

Methods details

Whole-mount immunofluorescence—All embryos were dissected in cold 1X PBS and fixed in 4% paraformaldehyde (PFA) at 4 °C with shaking for 1 h. Embryos were then washed twice (10 min each wash) with PBS at room temperature with shaking before dissection for whole-mount immunostaining. Whole hearts were washed in 0.5% PBT (1X PBS with 0.5% -Triton-X 100) at room temperature for one hour before incubation with primary antibodies. Primary antibodies were dissolved in blocking solution consisting of 5% donkey serum in 0.5% PBT. Hearts were incubated in the solution with primary antibodies with shaking overnight at 4 °C. Hearts were then washed every hour with 0.5% PBT for six hours with shaking at room temperature. Hearts were then stained with corresponding fluorescent-dye-conjugated secondary antibody secondary antibodies with the same conditions and procedure as for primary antibodies. After washing off the secondary antibodies with several washes of 0.5% PBT, hearts were transferred to 50% glycerol for 1 h and then mounted in anti-fade mounting media solution containing 100% glycerol + 20%(w/v) n-propyl gallate (Sigma P3130). Imaging was performed using Zeiss LSM-700 confocal microscope (10× or 20× objective lens) with Zen 2010 software (Zeiss). All antibodies used are listed in Key Resource Table.

Immunofluorescence on paraffin sections—Neonatal hearts were fixed in 4% PFA for 24 hours at 4°C, washed three times with PBS, dehydrated through increasing concentration of ethanol, cleared with xylene, and finally embedded in paraffin. Hearts were then sectioned at 10p.m. Hearts sectioned were dewaxed and rehydrated followed by antigen retrieval in preheated Sodium Citrate solution (pH= 6). The slides were then cooled down on ice and permeabilized using 0.5% PBT for 15 minutes at room temperature with agitation. Slides were washed with 1X PBS and incubated with a blocking solution (5% Donkey serum, 0.3% Tween-20, 20mM MgCl2 in 1X PBS) for 1 hour at room temperature. Primary antibodies, diluted in above mentioned blocking solution, were incubate O/N at 4°C. The following day, slides were washed in 1X PBS and incubated with corresponding fluorescent-dye-conjugated secondary antibodies (5% BSA in 1X PBS) for 1 hour at room temperature. Next, slides were washed in 1X PBS, stained with DAPI for 15 minutes at room temperature, washed again with 1X PBS and mounted in Fluoromount G (Southern Biotech; Cat: 0100–01) prior to confocal imaging.

Immunofluorescence on cryosections—Embryonic or neonatal hearts were fixed in 4% PFA for 1 hour at 4°C, washed in 1X PBS and dehydrated in 30% sucrose solution at

4°C O/N. The following day, hearts were embedded in OCT (Optical Cutting Temperature Compound, Fischer Health Care, Catalog: 4585), and stored at −80°C. 20pm cryosections were thawed at room temperature for 15 minutes followed by two consecutive washes in 0.5% PBT and incubated in blocking solution (5% Donkey serum, 0.5% PBT) for 1 hour. Primary antibodies were incubated at 4°C O/N. The following day, the slides were washed in 0.5% PBT, and incubated with corresponding fluorescent-dye-conjugated secondary antibody for 2–3 hours at room temperature followed by washes in 0.5% PBT. Cryosections were then mounted in Fluromount G prior to confocal imaging. For Cxcr4, staining was performed using Cy3 or fluorescein tyramide signal amplification (TSA, Perkin Elmer, Catalog: NEL701A001KT or NEL701A001KT).

In situ hybridization—*In-situ hybridization* for detection of *Cxcl12* transcript was performed on paraffin sections as previously described [42] Fluorescent *in-situ hybridization* (FISH) for detection of *Npr3* and *Cldn5* was performed as in Koop et al., 1996 with a modification to develop the fluorescent signal. Briefly, after hybridization, sections were incubated overnight at 4°C with anti-DIG POD (Millipore Sigma #11207733910). The next day, sections were washed 4 × 1 hr in 1× MABT. Finally, sections were washed for 3 × 10 min with 0.1 M borate buffer pH 8.5 and stained with tyramide signal amplification (TSA, Perkin Elmer, Catalog: NEL701A001KT). Sections were then washed in 1× P BS to remove the excess of fluorescent tyramide and antibodies were detected using the same immunofluorescent protocol for paraffin sections as described above.

Neonatal LCA ligation—This procedure was adopted from Mahmoud et al. [43]. Briefly: P4 neonatal mice were gently wrapped in two layers of surgical gauze and placed on ice for 6 minutes to induce hypothermic circulatory arrest. Neonates were then orientated in a supine position on a cold pack covered with a plastic wrap. Before surgery, thoracic area was disinfected with iodine followed by 70% ethanol. Left anterolateral thoracotomy was made under dissecting microscope guidance. Dissection was carried through the pectoralis major and minor muscles, and the thoracic cavity was opened via the 4th intercostal space. The left coronary artery was identified and ligated using 8–0 prolene suture. The chest was then closed in layers with interrupted 7–0 prolene sutures. For AAVs related experiments, 50ml of rAAVs were injected into the thoracic cavity with an insulin syringe immediately after surgery. Neonates were then allowed to recover at 37°C warm plate and, when conscious, returned to its mother's care. Due to mouse genetic inheritance, values for each parameter were compiled from both males and females from multiple litters.

Production of AAVs—Gibson Assembly cloning method was used to insert a 2A peptide coding sequence immediately before the full-length of murine *Bmp2* (SinoBiological, Cat.: MG51115-G, NM_007553.2) and subsequently subcloned into pENN.AAV.cTNT.PI.eGFP.WPRE serotype 9 adenoviral vector (Addgene, Cat.: #105543). A modified protocol from Wakimoto et al. was used to produces AAVs [44] HEK293T cells were transiently transfected with adenoviral helper plasmid pAdDeltaF6 (Addgene, Cat.:112867), trans-plasmid encoding AAV replicase and capsid gene pAAV2/9 (Addgene, Cat.:112865) and either pAAV-cTnT-GFP (vehicle) or pAAV-cTnT-GFP-p2A-Bmp2 vectors. 48–72hrs post-transfection, cells were harvested and centrifugated. AAVs particles were

then purify from AAV-producing cells using AAVpro Purification Kit Maxi (Takara, Cat. #6666). AAV titer from each sample was measured by Droplet Digital PCR (ddPCR).

Embryonic ventricular explants—Ventricular explants were performed following modified version of the protocol from Large et al. [45]. The experiment was performed three times. E10.5 ventricles from each embryo were dissected in sterile 1X PBS and gently placed onto a cell culture insert (EMD Millipore, Cat. PI8P01250) coated with Matrigel (Corning, Cat. 354230). Two explants for each condition were located to the center of the insert. Excess of 1X PBS was removed and 200 pl of endothelial cell growth basal media (EBM-Cat. CC-3156) supplemented with 2% FBS (HyClone, Cat. SH3007003IR) were added to the space between the insert and the well. Explants were then covered with extra 100 pl of 2% FBS basal media. Ventricles were cultured in these conditions at 37 °C for 16 h. The day after, explants were washed with 1X PBS and recombinant rBMP2 (R&D Systems, Cat. 355-BM-010) or rVegfa (PeproTech, Cat. 450–32) diluted in 2% FBS basal media was added to the explants individually or in a 1:1 mixture at a final concentration of 20ug/ml. Explants cultured only with 2% FBS basal media represented vehicle controls. at 37 °C for approximately 4 days in basal media or experimental conditions basal media was replaced. Explants were incubated at 37°C for 4 days replacing media every 24 hours. Finally, explants were washed with 1X PBS and fixed in 4% PFA for 10 min at 4 °C.

***In vivo* inhibition of Bmp signaling—**BMP inhibitor (LDN-193189 Cat. SML0559–5MG) was administrated via intraperitoneal injections into pregnant females at E10.5 and E11.5. LDN-193189 was dissolved in endotoxin-free water (Sigma-Aldrich, 95289) at 1.5 mg/ml and neutralised at pH 6.8. The amount of LDN-193189 per injection was 6 mg/kg. Control females received an equivalent volume of steril 1X PBS via intraperitoneal injections. Embryos were collected at E12.5 and fixed for whole-mount immunostaining analysis, as described above.

Single-cell RNA sequencing protocol

Tissue Dissociation and Sample Preparation: *BmxCreERT2;Rosa*$^{tdTomato/tdTomato}$*;Cxcr4*$^{lox/+}$ males were crossed to *;Cxcr4*$^{lox/f1ox}$ females, which were dosed with tamoxifen at E9.5.
E17.5 embryos from two litters were harvested in cold, sterile 1X PBS.
Three *BmxCreERT2;Rosa*$^{tdTomato/tdTomato}$*;Cxcr4*$^{lox/+}$ (heterozygous, controls) and five *BmxCreERT2;Rosa*$^{tdTomato/tdTomato}$*;Cxcr4*$^{flox/+}$ (mutants) embryos were identified by genomic PCR using Cre; Cxcr4flox and tdTomato primers. Hearts were isolated and dissected to remove the atria, pulmonary and aortic valves. Hearts were then dissociated in a 600 µl mix consisting of 500 U/ml collagenase IV (Worthington #LS004186), 1.2 U/ml dispase (Worthington #LS02100), 32 U/ml DNase I (Worthington #LS002007), and sterile DPBS with Mg^{2+} and Ca^{2+} at 37 degrees for 45 min and resuspended by pipetting every 5 min. Once digestion was complete, 5 ml of a cold 5% FBS in 1× PBS mixture was added and the suspension was filtered through a 40 µm strainer. After further rinsing the strainer with 5 ml of 5% FBS/PBS, the cell suspension was centrifuged at 400 g at 4°C for 5 min. The cells were washed and resuspended once more in 1 ml 5% FBS/PBS. The following antibodies were added at the concentration of 1:50 and incubated on ice for 45

min: APC/Cy7 Cd45 (Biolegend #103116), APC Pecam1 (Biolegend #102410), APC/Cy7 Ter-119 (Biolegend #116223). DAPI (1.1 μM) was added to the cells immediately before FACS. Once stained, the cells were sorted on a Sony MA900 cell sortrer into 1.5 ml tubes. The gates were set up to sort cells with low DAPI, low Cd45 (hematopoietic cells), low Ter119 (erythroid cells), high Pecam1 (endothelial marker), and either high or low PE-Texas Red *(tdTomato* positive or negative). Compensation controls were set up for each single channel (PE-Texas Red, APC, APC/Cy7) before sorting the final cells. The samples were then submitted to the Stanford Genome Sequencing Service Center for 10* single-cell v3.1 3' library preparation. For each genotype, libraries from the tdTomato-positive were pooled and sequencing was performed on two lanes of an Illumina NovaSeq 6000 SP flow cell. Tissue dissection and sample preparation for E12 and E17.5 *BmxCreERT2;Rosa*^{tdTomato} hearts was performed as described by Phansalkar et al [29]

Processing of sequencing data: Raw Illumina reads for all datasets were demultiplexed and converted to FASTQ using bcl2fastq (Illumina). Reads were aligned to GRCm38 Ensembl release 81 as well tdTomato sequences and a gene count matrix was obtained using Cell Ranger v3.1.0 (10× Genomics).

Processing of count data: The majority of scRNAseq data analysis was performed using R and Seurat v3 [46] and v4 [39]. Cells were deemed low-quality and excluded from downstream analysis if they expressed less than 1000 genes or if more than 10% of reads aligned to mitochondrial genes. For all datasets, non-endothelial subtypes (e.g., blood and immune cells, cardiomyocytes, smooth muscle, fibroblasts) as well as a small number of lymphatic cells were removed.

Normalization, variable feature selection, scaling, and dimensionality reduction using principal component analysis were performed using the standard Seurat v3 and v4 pipeline. Technical variables genes per cell, reads per cell, cell cycle and mitochondrial read percentage were regressed out in the ScaleData function. Following this, construction of a shared nearest neighbour graph, cluster identification with the Louvain algorithm[46], and Uniform Manifold Approximation and Projection (UMAP) dimensionality reduction [47] were performed using FindNeighbors (dims = 1:25), FindClusters (res=0.8), and RunUMAP (dims = 1:25) functions in Seurat.

A subset of ECs from E12 was used for further analysis (integration, trajectory and ligand-receptor interaction analysis): the endo EC clusters closest to CV ECs in the UMAP (E1 and E4), the SV cluster, and the CV clusters (CV1 and CV2). The VE cluster in E17.5 was excluded for the data integration and trajectory analysis. Endo, vein and cycling CV ECs were removed from the integrated *Cxcr4*$^{flox+}$ and *Cxcr4*$^{fox/flox}$ dataset Differential expression testing Differential gene expression testing in Fig. 5G was performed with the FindMarkers function in Seurat with the following parameters: logfc.threshold = 0.3, min.pct = 0.2 and filtered for p-value < 0.001.

Datasets integration: After QC filtering, the samples were normalized, scaled and centred, 5,000 shared highly variable genes were identified using Seurat FindVariableFeatures and SelectIntegrationFeatures() functions. Integration anchors were identified based on these

genes using canonical correlation analysis as implemented in the FindIntegrationAnchors () function with the following settings: reduction = "cca",dims = 1:5, k.anchor = 20. The data were then integrated using IntegrateData() and scaled again using ScaleData(). PCA and UMAP with 30 principal components were performed. A nearest- neighbour graph using the 30 dimensions of the PCA reduction was calculated using FindNeighbours(), followed by clustering using FindClusters() with a resolution of 0.5. Same parameters have been used to perform integration all Endo ECs (Suppl. Figure 6E) and capillary cells (Suppl. Figure 6F) from E12 and E17.5.

Trajectory analysis: We used the Bioconductor package Slingshot [31], Dynverse [48] within ASC Seurat web application [49] to determine pseudotime lineage trajectories and identify top 50 genes DEG along the trajectory. CytoTRACE (Cellular (Cyto) Trajectory Reconstruction Analysis using gene Counts and Expression) [37] to predict the differentiation state of the cells in the selected E12 and E17.5 clusters with default parameters.

Ligand-receptor interaction analysis: For ligand-receptor analysis, we used CellChat [40] (https://github.com/sqjin/CellChat) v1.1 using the SecretedSignaling subset of the mouse CellChatDB, with default parameters.

Quantification and statistical analysis

Quantification of tdTomato expressing cells in ECs (tdTomato$^+$-Erg$^+$ cells) was performed from different z-stack in whole-mount images or heart sections at different time points. Total number of Erg+ cells was automatically calculated using Image-based Tool for Counting Nuclei (ITCN) plugin in FIJI whereas tdTomato+ cells were manually counted using the CellCounter plugin. In Fig. 1F and 6H, endo derived CVs contribution is represented as ratio between total number of tdTomato+ cells and Vegr2 or IB4 vessel area measured using the AnalyzeParticle plugin in FIJI.

Colocalizaton images were produced using the "analyze particles" plugin in FIJI on masks of GFP+ nuclei and ERG+ nuclei chosen from a default threshold with parameters of circularity >.2 and area > 75 pixels. The two masks were combined using the AND function in the ROI manager and the resulting pixels were overlaid on the TD-Tomato expressing channel. Statistical analysis and graphs were generated using Prism 9 (GraphPad). All statistical tests were performed using two-sided, unpaired Student's t-tests except. *P < 0.05, **P < 0.01, ***P < 0.001 and **** P ≤ 0.0001. Sample size was chosen empirically according to previous experience in the calculation of experimental variability. No statistical method was used to predetermine sample size. All experiments were carried out with at least three biological replicates. Numbers of animals used, and statistical significance are described in the corresponding figure legends.

Supplementary Material

Refer to Web version on PubMed Central for supplementary material.

Acknowledgements

Grant support: K.R.-H., NIH/NHLBL (R01-HL128503); G.D., EMBO (ALTF 1542-2016) and NIH (T32HL120824); R.P., AHA graduate fellowship; P.E.R.C, NIGMS (NIH T32GM007276) and NSF-GRFP (DGE-1656518); Stanford Genome Sequencing Services Center, NIH (S100D020141). We thank Ralf Adams for *BmxCreER,* José Luis de la Pompa for *ISH* reagents, Rahul Sinha for experimental assistance, and all members of the Red-Horse lab for technical and intellectual support.

Inclusion and Diversity

We support inclusive, diverse and equitable conduct of research

References

1. Dunbar SB, Khavjou OA, Bakas T, Hunt G, Kirch RA, Leib AR, Morrison RS, Poehler DC, Roger VL, and Whitsel LP (2018). Projected Costs of Informal Caregiving for Cardiovascular Disease: 2015 to 2035: A Policy Statement From the American Heart Association. Circulation 137, e558–e577. 10.1161/cir.0000000000000570. [PubMed: 29632217]
2. Ylä-Herttuala S, Bridges C, Katz MG, and Korpisalo P. (2017). Angiogenic gene therapy in cardiovascular diseases: dream or vision? Eur Heart J 38, 1365–1371. 10.1093/eurheartj/ehw547. [PubMed: 28073865]
3. Red-Horse K, Ueno H, Weissman IL, and Krasnow MA (2010). Coronary arteries form by developmental reprogramming of venous cells. Nature 464, 549–553. 10.1038/nature08873. [PubMed: 20336138]
4. Wu B, Zhang Z, Lui W, Chen X, Wang Y, Chamberlain AA, Moreno-Rodriguez RA, Markwald RR, O'Rourke BP, Sharp DJ, et al. (2012). Endocardial cells form the coronary arteries by angiogenesis through myocardial-endocardial VEGF signaling. Cell 151, 1083–1096. 10.1016/j.cell.2012.10.023. [PubMed: 23178125]
5. Chen HI, Sharma B, Akerberg BN, Numi HJ, Kivelä R, Saharinen P, Aghajanian H, McKay AS, Bogard PE, Chang AH, et al. (2014). The sinus venosus contributes to coronary vasculature through VEGFC-stimulated angiogenesis. Development 141, 4500–4512. 10.1242/dev.113639 PMID - 25377552. [PubMed: 25377552]
6. Tian X, Hu T, Zhang H, He L, Huang X, Liu Q, Yu W, He L, Yang Z, Zhang Z, et al. (2013). Subepicardial endothelial cells invade the embryonic ventricle wall to form coronary arteries. Cell Res 23, 1075–1090. 10.1038/cr.2013.83. [PubMed: 23797856]
7. Tian X, Hu T, Zhang H, He L, Huang X, Liu Q, Yu W, He L, Yang Z, Yan Y, et al. .(2014). Vessel formation. De novo formation of a distinct coronary vascular population in neonatal heart. Science 345, 90–94. 10.1126/science.1251487. [PubMed: 24994653]
8. Sharma B, Ho L, Ford GH, Chen HI, Goldstone AB, Woo YJ, Quertermous T, Reversade B, and Red-Horse K. (2017). Alternative Progenitor Cells Compensate to Rebuild the Coronary Vasculature in Elabela- and Apj-Deficient Hearts. Dev Cell 42, 655–666.e653. 10.1016/j.devcel.2017.08.008 PMID - 28890073. [PubMed: 28890073]
9. Su T, Stanley G, Sinha R, D'Amato G, Das S, Rhee S, Chang AH, Poduri A, Raftrey B, Dinh TT, et al. (2018). Single-cell analysis of early progenitor cells that build coronary arteries. Nature 559, 356–362. 10.1038/s41586-018-0288-7 PMID - 29973725. [PubMed: 29973725]
10. Zhang H, Pu W, Li G, Huang X, He L, Tian X, Liu Q, Zhang L, Wu SM, Sucov HM, and Zhou B. (2016). Endocardium Minimally Contributes to Coronary Endothelium in the Embryonic Ventricular Free Walls. Circ Res 118, 1880–1893. 10.1161/circresaha.116.308749. [PubMed: 27056912]
11. Sharma B, Ho L, Ford GH, Chen HI, Goldstone AB, Woo YJ, Quertermous T, Reversade B, and Red-Horse K. (2017). Alternative Progenitor Cells Compensate to Rebuild the Coronary Vasculature in Elabela- and Apj-Deficient Hearts. Dev Cell 42, 655–666.e653. 10.1016/j.devcel.2017.08.008. [PubMed: 28890073]
12. Chen HI, Sharma B, Akerberg BN, Numi HJ, Kivelä R, Saharinen P, Aghajanian H, McKay AS, Bogard PE, Chang AH, et al. (2014). The sinus venosus contributes to coronary vasculature

through VEGFC-stimulated angiogenesis. Development 141, 4500–4512. 10.1242/dev.113639. [PubMed: 25377552]

13. Neal A, Nornes S, Payne S, Wallace MD, Fritzsche M, Louphrasitthiphol P, Wilkinson RN, Chouliaras KM, Liu K, Plant K, et al. (2019). Venous identity requires BMP signalling through ALK3. Nat Commun 10, 453. 10.1038/s41467-019-08315-w. [PubMed: 30692543]
14. Rhee S, Chung JI, King DA, D'Amato G, Paik DT, Duan A, Chang A, Nagelberg D, Sharma B, Jeong Y, et al. (2018). Endothelial deletion of Ino80 disrupts coronary angiogenesis and causes congenital heart disease. Nat Commun 9, 368. 10.1038/s41467-017-02796-3. [PubMed: 29371594]
15. Sharma B, Chang A, and Red-Horse K. (2017). Coronary Artery Development: Progenitor Cells and Differentiation Pathways. Annu Rev Physiol 79, 1–19. 10.1146/annurev-physiol-022516-033953. [PubMed: 27959616]
16. Zhang H, Lui KO, and Zhou B. (2018). Endocardial Cell Plasticity in Cardiac Development, Diseases and Regeneration. Circ Res 122, 774–789. 10.1161/circresaha.117.312136. [PubMed: 29496799]
17. Su T, Stanley G, Sinha R, D'Amato G, Das S, Rhee S, Chang AH, Poduri A, Raftrey, Dinh TT, et al. (2018). Single-cell analysis of early progenitor cells that build coronary arteries. Nature 559, 356–362. 10.1038/s41586-018-0288-7. [PubMed: 29973725]
18. Lu P, Wang Y, Liu Y, Wang Y, Wu B, Zheng D, Harvey RP, and Zhou B. (2021). Perinatal angiogenesis from pre-existing coronary vessels via DLL4-NOTCH1 signalling. Nature Cell Biology 23, 967–977. 10.1038/s41556-021-00747-1. [PubMed: 34497373]
19. Tang J, Zhang H, He L, Huang X, Li Y, Pu W, Yu W, Zhang L, Cai D, Lui KO, and Zhou B. (2018). Genetic Fate Mapping Defines the Vascular Potential of Endocardial Cells in the Adult Heart. Circ Res 122, 984–993. 10.1161/circresaha.117.312354. [PubMed: 29374073]
20. Rasanen M, Sultan I, Paech J, Hemanthakumar KA, Yu W, He L, Tang J, Sun Y, Hlushchuk R, Huan X, et al. (2021). VEGF-B Promotes Endocardium-Derived Coronary Vessel Development and Cardiac Regeneration. Circulation 143, 65–77. 10.1161/circulationaha.120.050635. [PubMed: 33203221]
21. Jiang Z, Lu Z, Kou S, Feng T, Wei Y, Gao Z, Deng D, Meng J, Lin CP, Zhou B, and Zhang H. (2021). Overexpression of Kdr in adult endocardium induces endocardial neovascularization and improves heart function after myocardial infarction. Cell Res 31, 485–487. 10.1038/s41422-020-00436-y. [PubMed: 33219343]
22. Ehling M, Adams S, Benedito R, and Adams RH (2013). Notch controls retinal blood vessel maturation and quiescence. Development 140, 3051–3061. 10.1242/dev.093351. [PubMed: 23785053]
23. Mikawa T, and Fischman DA (1992). Retroviral analysis of cardiac morphogenesis: discontinuous formation of coronary vessels. Proc Natl Acad Sci U S A 89, 9504–9508. 10.1073/pnas.89.20.9504. [PubMed: 1409660]
24. Harrison MR, Bussmann J, Huang Y, Zhao L, Osorio A, Burns CG, Burns CE, Sucov HM, Siekmann AF, and Lien CL (2015). Chemokine-guided angiogenesis directs coronary vasculature formation in zebrafish. Dev Cell 33, 442–454. 10.1016/j.devcel.2015.04.001. [PubMed: 26017769]
25. Cavallero S, Shen H, Yi C, Lien CL, Kumar SR, and Sucov HM (2015). CXCL12 Signaling Is Essential for Maturation of the Ventricular Coronary Endothelial Plexus and Establishment of Functional Coronary Circulation. Dev Cell 33, 469–477. 10.1016/j.devcel.2015.03.018. [PubMed: 26017771]
26. Kono M, Tucker AE, Tran J, Bergner JB, Turner EM, and Proia RL (2014). Sphingosine-1-phosphate receptor 1 reporter mice reveal receptor activation sites in vivo. J Clin Invest 124, 2076–2086. 10.1172/jci71194. [PubMed: 24667638]
27. Engelbrecht E, Levesque MV, He L, Vanlandewijck M, Nitzsche A, Niazi H, Kuo A, Singh SA, Aikawa M, Holton K, et al. (2020). Sphingosine 1-phosphate-regulated transcriptomes in heterogenous arterial and lymphatic endothelium of the aorta. Elife 9. 10.7554/eLife.52690.
28. Tumbar T, Guasch G, Greco V, Blanpain C, Lowry WE, Rendl M, and Fuchs E. (2004). Defining the epithelial stem cell niche in skin. Science 303, 359–363. 10.1126/science.1092436. [PubMed: 14671312]

29. Phansalkar R, Krieger J, Zhao M, Kolluru SS, Jones RC, Quake SR, Weissman I, Bernstein D, Winn VD, D'Amato G, and Red-Horse K. (2021). Coronary blood vessels from distinct origins converge to equivalent states during mouse and human development. Elife 10. 10.7554/eLife.70246.
30. Kalucka J, de Rooij L, Goveia J, Rohlenova K, Dumas SJ, Meta E, Conchinha NV, Taverna F, Teuwen LA, Veys K, et al. (2020). Single-Cell Transcriptome Atlas of Murine Endothelial Cells. Cell 180, 764–779.e720. 10.1016/j.cell.2020.01.015. [PubMed: 32059779]
31. Street K, Risso D, Fletcher RB, Das D, Ngai J, Yosef N, Purdom E, and Dudoit S. (2018). Slingshot: cell lineage and pseudotime inference for single-cell transcriptomics. BMC Genomics 19, 477. 10.1186/s12864-018-4772-0. [PubMed: 29914354]
32. Ma L, Lu MF, Schwartz RJ, and Martin JF (2005). Bmp2 is essential for cardiac cushion epithelial-mesenchymal transition and myocardial patterning. Development 132, 5601–5611. 10.1242/dev.02156. [PubMed: 16314491]
33. Rivera-Feliciano J, and Tabin CJ (2006). Bmp2 instructs cardiac progenitors to form the heart-valve-inducing field. Dev Biol 295, 580–588. 10.1016/j.ydbio.2006.03.043. [PubMed: 16730346]
34. Luna-Zurita L, Prados B, Grego-Bessa J, Luxan G, del Monte G, Benguria A, Adams RH, Perez-Pomares JM, and de la Pompa JL (2010). Integration of a Notch-dependent mesenchymal gene program and Bmp2-driven cell invasiveness regulates murine cardiac valve formation. J Clin Invest 120, 3493–3507. 10.1172/jci42666. [PubMed: 20890042]
35. Prados B, Gomez-Apinaniz P, Papoutsi T, Luxan G, Zaffran S, Perez-Pomares JM, and de la Pompa JL (2018). Myocardial Bmp2 gain causes ectopic EMT and promotes cardiomyocyte proliferation and immaturity. Cell Death Dis 9, 399. 10.1038/s41419-018-0442-z. [PubMed: 29540665]
36. Papoutsi T, Luna-Zurita L, Prados B, Zaffran S, and de la Pompa JL (2018). Bmp2 and Notch cooperate to pattern the embryonic endocardium. Development 145. 10.1242/dev.163378.
37. Gulati GS, Sikandar SS, Wesche DJ, Manjunath A, Bharadwaj A, Berger MJ, Ilagan F, Kuo AH, Hsieh RW, Cai S, et al. (2020). Single-cell transcriptional diversity is a hallmark of developmental potential. Science 367, 405–411. 10.1126/science.aax0249. [PubMed: 31974247]
38. Ivins S, Chappell J, Vernay B, Suntharalingham J, Martineau A, Mohun TJ, and Scambler PJ (2015). The CXCL12/CXCR4 Axis Plays a Critical Role in Coronary Artery Development. Dev Cell 33, 455–468. 10.1016/j.devcel.2015.03.026. [PubMed: 26017770]
39. Hao Y, Hao S, Andersen-Nissen E, Mauck WM 3rd, Zheng S, Butler A, Lee MJ, Wilk AJ, Darby C, Zager M, et al. (2021). Integrated analysis of multimodal single-cell data. Cell 184, 3573–3587.e3529. 10.1016/j.cell.2021.04.048. [PubMed: 34062119]
40. Jin S, Guerrero-Juarez CF, Zhang L, Chang I, Ramos R, Kuan CH, Myung P, Plikus MV, and Nie Q. (2021). Inference and analysis of cell-cell communication using CellChat. Nat Commun 12, 1088. 10.1038/s41467-021-21246-9. [PubMed: 33597522]
41. Pereira WJ, Almeida FM, Conde D, Balmant KM, Triozzi PM, Schmidt HW, Dervinis C. Pappas GJ Jr., and Kirst M. (2021). Asc-Seurat: analytical single-cell Seurat-based web application. BMC Bioinformatics 22, 556. 10.1186/s12859-021-04472-2. [PubMed: 34794383]
42. Koop KE, MacDonald LM, and Lobe CG (1996). Transcripts of Grg4, a murine groucho-related gene, are detected in adjacent tissues to other murine neurogenic gene homologues during embryonic development. Mech Dev 59, 73–87. 10.1016/0925-4773(96)00582-5. [PubMed: 8892234]
43. Mahmoud AI, Porrello ER, Kimura W, Olson EN, and Sadek HA (2014). Surgical models for cardiac regeneration in neonatal mice. Nat Protoc 9, 305–311. 10.1038/nprot.2014.021. [PubMed: 24434799]
44. Wakimoto H, Seidman JG, Foo RSY, and Jiang J. (2016). AAV9 Delivery of shRNA to the Mouse Heart. Curr Protoc Mol Biol 115, 23.16.21–23.16.29. 10.1002/cpmb.9.
45. Large CL, Vitali HE, Whatley JD, Red-Horse K, and Sharma B. (2020). In Vitro Model of Coronary Angiogenesis. J Vis Exp. 10.3791/60558.
46. Stuart T, Butler A, Hoffman P, Hafemeister C, Papalexi E, Mauck WM 3rd, Hao Y, Stoeckius M, Smibert P, and Satija R. (2019). Comprehensive Integration of Single-Cell Data. Cell 177, 1888–1902.e1821. 10.1016/j.cell.2019.05.031. [PubMed: 31178118]

47. Becht E, Mclnnes L, Healy J, Dutertre CA, Kwok IWH, Ng LG, Ginhoux F, and Newell EW (2018). Dimensionality reduction for visualizing single-cell data using UMAP. Nat Biotechnol. 10.1038/nbt.4314.

48. Saelens W, Cannoodt R, Todorov H, and Saeys Y. (2019). A comparison of single-cell trajectory inference methods. Nat Biotechnol 37, 547–554. 10.1038/s41587-019-0071-9. [PubMed: 30936559]

49. Pereira W, Almeida F, Balmant K, Rodriguez D, Triozzi P, Schmidt H, Dervinis C, Pappas G, and Kirst M. (2021). Asc-Seurat - Analytical single-cell Seurat-based web application. bioRxiv, 2021.2003.2019.436196. 10.1101/2021.03.19.436196.

Highlights

- Endocardium gives rise to coronary vessels primarily at mid-gestation development
- Bmp2 stimulates VegfA-dependent coronary angiogenesis from endocardium
- Bmp2 overexpression reactivates endocardial angiogenesis in injured neonatal heart
- Cxcl12/Cxcr4 signaling mediates endocardium-derived artery morphogenesis

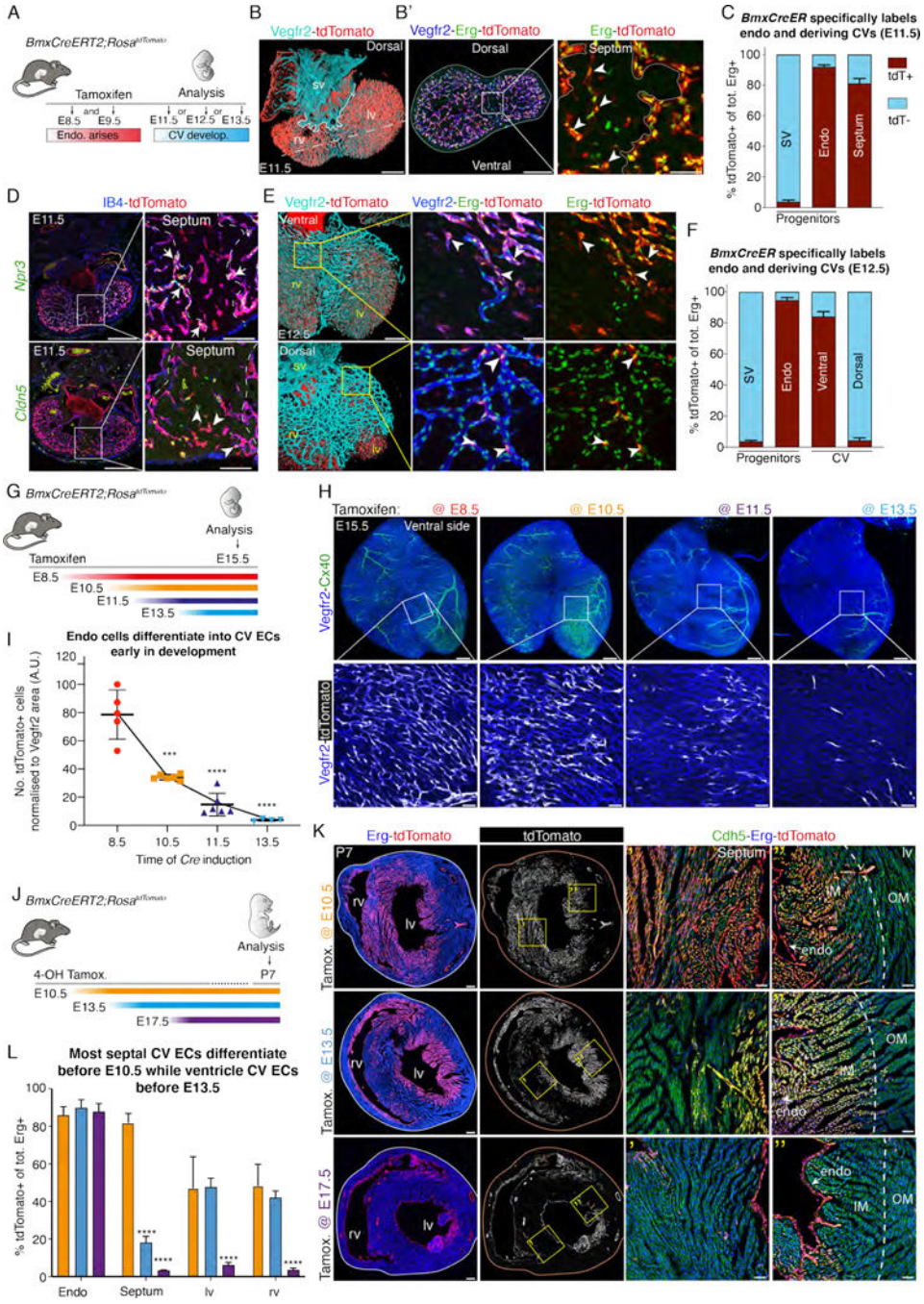

Figure 1. Endocardial-derived coronary vessels arose early in development, first in the septum then inner free walls.

A) Experimental strategy for **B-E. B)** Whole-mount dorsal view of E11.5 *BmxCreERT2;Rosa*^{tdTomato} lineage-labeled heart. Solid line demarcates SV-derived ECs. Dotted line indicates section in **B'. B')** Box highlights septum and first endo-derived CVs (arrowheads). C) Quantification from n=4 heart tissue sections. **D) FISH** labels endo *(Npr3)* and CV ECs *(Cldn5).* Arrows and arrowheads indicate IB4+; tdTomato+ endo and endo-derived CV ECs, respectively. **E)** Confocal images of *BmxCreERT2;Rosa*^{tdTomato} hearts.

Arrowheads indicate endo-derived CVs on the ventral and dorsal sides. **F)** Quantification from n=6 whole-mount hearts. **G)** Experimental strategy for **H** and **I. H)** Whole-mount images of *BmxCreERT2;Rosa*^{tdTomato} hearts immunostained for Vegfr2 and the arterial marker Cx40. Boxed regions highlight a reduction of endo-derived CVs (tdTomato+, white cells) from early vs. later Cre inductions. **I)** Quantification where each symbol indicates an individual heart. **J)** Experimental strategy for **K** and **L. K)** Representative transverse heart sections. Boxed regions show endo contributions to septal and left ventricle (lv) CVs (tdTomato+, red cells). Dotted lines indicate border between inner (IM) and outer myocardium (OM). **L)** Quantification from tissues sections: E10.5, $n = 6$ hearts; E13.5, $n = 4$ hearts; E17.5, $n = 4$ hearts. Scale bar=200 μM in B, B', D, E, H and K (full view). Scale bar=50 μM in B', D, E, H and K (boxed regions). Data are mean ± s.d. ***P < 0.001, ****, P < 0.0001, by Student's t-test.

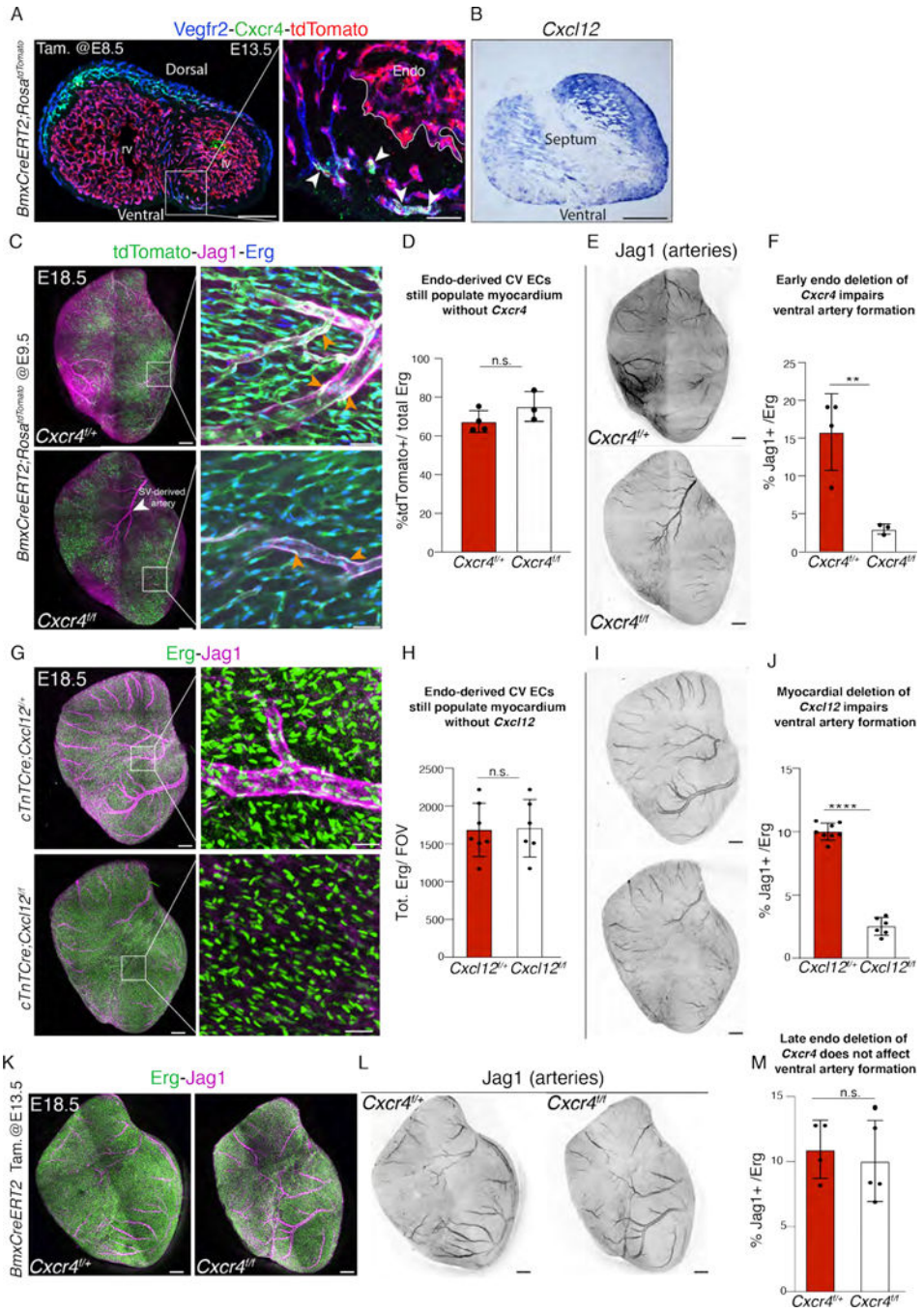

Figure 2. Cxcl12-Cxcr4 signaling was critical for artery formation rather than general endothelial migration.

A) Immunostaining of lineage-traced heart section. Arrowheads indicate endo-derived CV expressing Cxcr4. Endocardium (endo) lacks Cxcr4. **B)** *In* situ hybridization of *Cxcl12* (blue) in E14.5 WT heart section. **C** and **D)** Whole-mount ventral views **(C)** and quantification **(D)** of *BmxCreERT2;Rosa26tdTomato;Cxcr4*$^{f/+}$ (controls, n = 4 hearts) and *BmxCreERT2;Rosa26tdTomato;Cxcr4*$^{f/f}$ (mutants, n = 3 hearts) with early endocardial deletion of *Cxcr4. E* and **F**) Whole-mount views (**E**) and quantification (**F**) of arteries in

the hearts in **C**. **G-J**) Myocardial deletion of *Cxc12* recapitulates phenotype seen in **C-F.** *cTnTCre;CxcU2*$^{f/+}$ are controls with n= 6 hearts and *cTnTCre;Cxcl12*$^{f/f}$ are mutants with *n* = 6 hearts. **K-M**) Later endocardial deletion of *Cxcr4* does not affect arterial development. Scale bar=200 μM in A, B, C, E, G, I, K and L (full view). Scale bar=50 μM in A, C, and G (boxed regions). Data are mean ± s.d. **P ≤ 0.01, ****, p ≤ 0.0001, n.s., not significant, by Student's *t*-test.

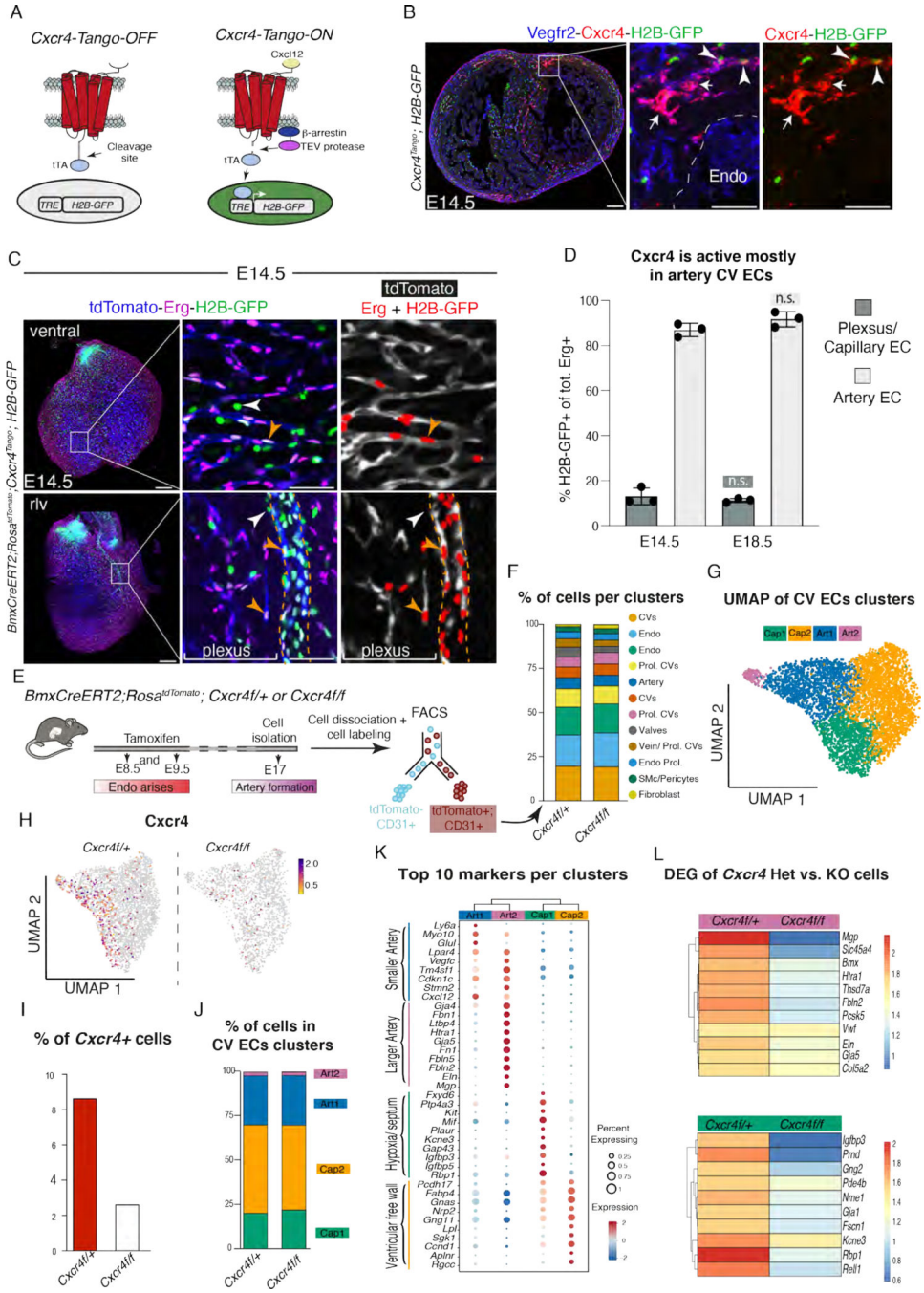

Figure 3. A new Cxcr4 activity reporter identified that most receptor activation is in artery endothelial cells.

A and **B)** Schematic representation of Cxcr4-Tango mouse system. **B)** Immunofluorescence on heart tissue sections. Cxcr4 expression in CV ECs was observed with (arrowheads) and without (arrows) Tango activity. **C)** Ventral and right lateral (rlv) view of whole mount, lineage labeled hearts. TdTomato+ endo-derived CV ECs colocalizedwith Tango activation (orange arrowheads) primarily in arteries (dotted lines) rather than plexus. White arrows indicate Cxcr4 activity in non-ECs. **D)** Quantification from n=3 hearts per stage.

E) Experimental scheme for scRNAseq in F-L. **F)** *Cxcr4* deletion does not affect the proportions of EC subtypes. **G)** UMAP plots of $Cxcr4^{fl/+}$ and $Cxcr4^{f/:fl}$ integrated datasets subsetted for CV ECs cells. **H** and **I)** Feature plots **(H)** and quantification **(I)** showing reduced number of *Cxcr4* expressing cells in *fl/fl* sample. **J)** Subtype percentages were not different among genotypes. **K)** Top marker genes allow more-specific identification of clusters based on published data (see text). **L)** Heatmaps showing normalized expression values (z-score) of the differentially expressed genes (DEG) between genotypes in Art2 (top) and Cap1 (bottom). Scale bar=200 μM in B and C (full view). Scale bar=50 μM in B and C (boxed regions). Data are mean ± s.d. n.s., not significant, by Student's *t*-test.

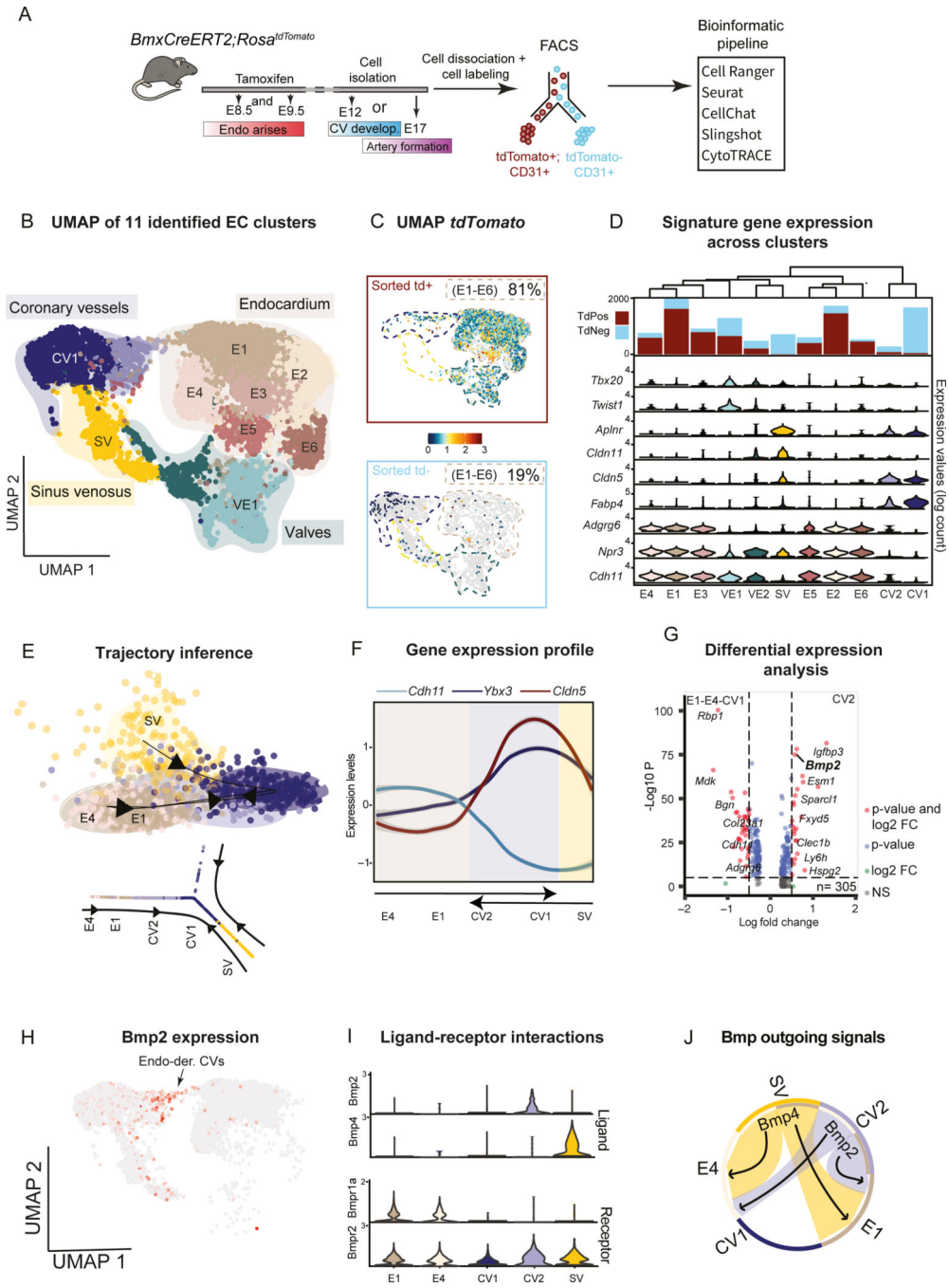

Figure 4. ScRNAseq of E12 cardiac ECs showed upregulation of Bmp2 signaling during endo-to-CV transition.

A) Experimental scheme for scRNAseq in Figures 4 and 5. **B)** UMAP plot of EC clusters grouped into the 4 indicated subtypes. **C.** UMAP with *tdTomato* expression in cells sorted as either *tdTomato* positive or negative. Dotted line colors are cluster identities from **B.** Percentages of total endo cells in each category are indicated. **D)** Bar plots indicating *tdTomato+* and *tdTomato−* cells in clusters and their order based on similarity (top tree). Violin plots show gene expression used for cluster identification. **E)** Visualization of the

trajectory inferred using slingshot on a dimensionality reduction of the cells (top panel) and as a 2D graph (bottom panel). **F)** Gene expression profile of 3 selected markers along the 2D trajectory from **E** (x *axis=cells*). **G)** Volcano plot showing differentially expressed genes between CV2 vs E1-E4 + CV1 clusters (cut-off for log2FC is >|2|; cut-off for P value is 10e-6). **H)** *Bmp2* expression is enriched in CVs transitioning from endo. **I)** Expression of ligand-receptors genes related to BMP signaling pathway. J) Chord plot showing all significant interactions associated with BMP signaling pathway.

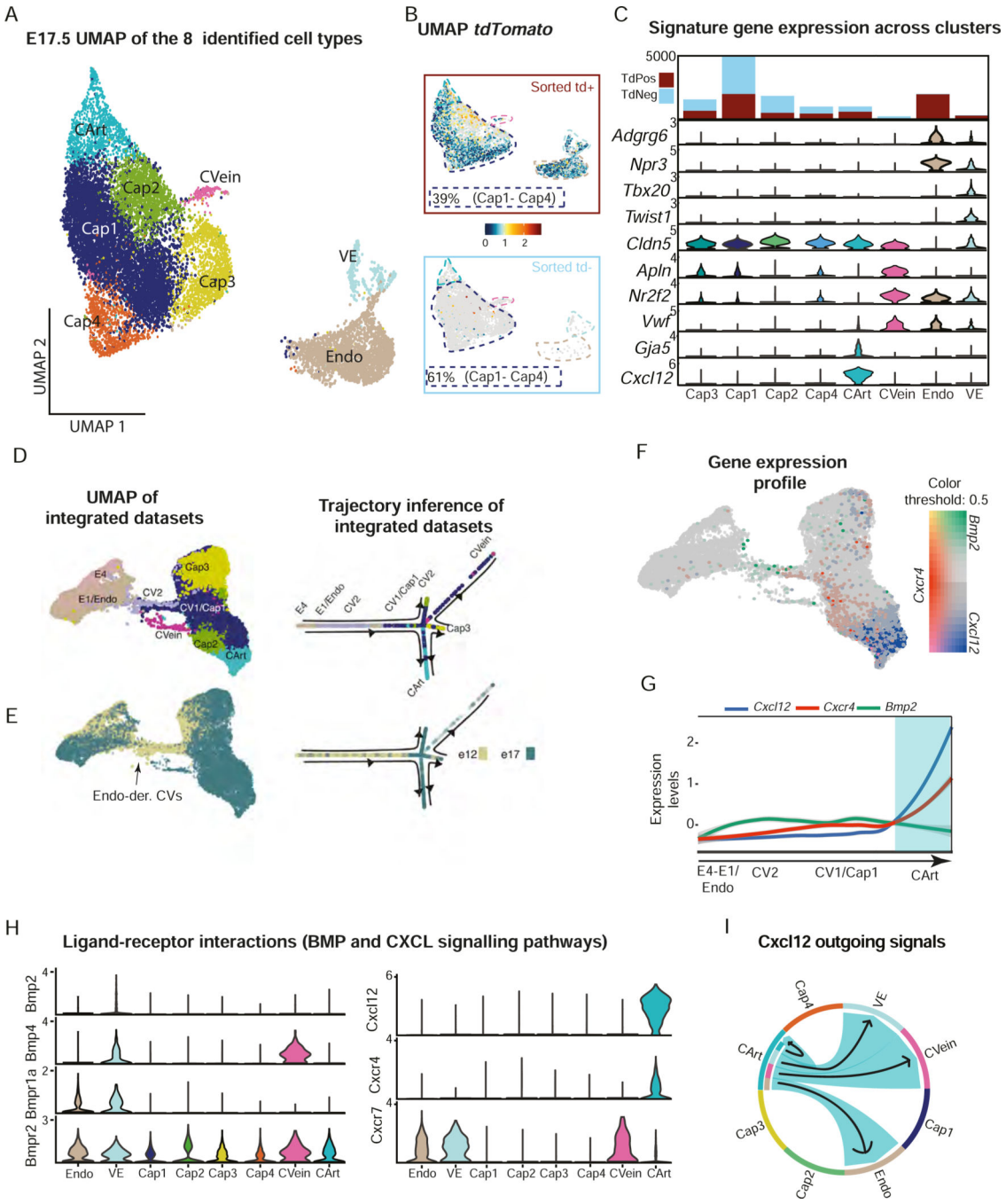

Figure 5. Combined E12 and E17.5 scRNAseq indicated the endo-to-CV transition and Bmp2 expression is largely restricted to the early time point.

A) UMAP plot of EC clusters from E17.5 grouped into 5 subtypes: Endo; Valve (VE); Coronary Capillary (Cap1-Cap4); Coronary Veins (CVein); Coronary Arteries (CArt). **B)** UMAP with *tdTomato* expression in cells sorted as either *tdTomato* positive or negative. Dotted line colors are cluster identities from **A**. Percentages of total capillaries in each category are indicated. **C)** Bar plots indicating *tdTomato+* and *tdTomato−* cells in clusters and their order based on similarity (top tree). Violin plots show gene expression used

for cluster identification. **D** and **E)** UMAP of E12/17.5 integrated dataset (left panel) and visualization of the trajectory as a 2D graph structure (right panel), colored according to clusters of origin **(D)** or developmental stage **(E). F)** UMAP of integrated dataset colored by expression of the 3 indicated genes. **G)** Gene expression profile of 3 markers along the 2D trajectory of integrated dataset (x axis= cells). **H)** Expression at E17.5 of genes related to Ligand-Receptors pairs of BMP (left) and CXCL (right) signaling pathways. Bmp2 is down, and *Cxcl12* is up. **I)** Chord plot showing all the significant interactions (L-R pairs) associated with CXCL signaling pathway.

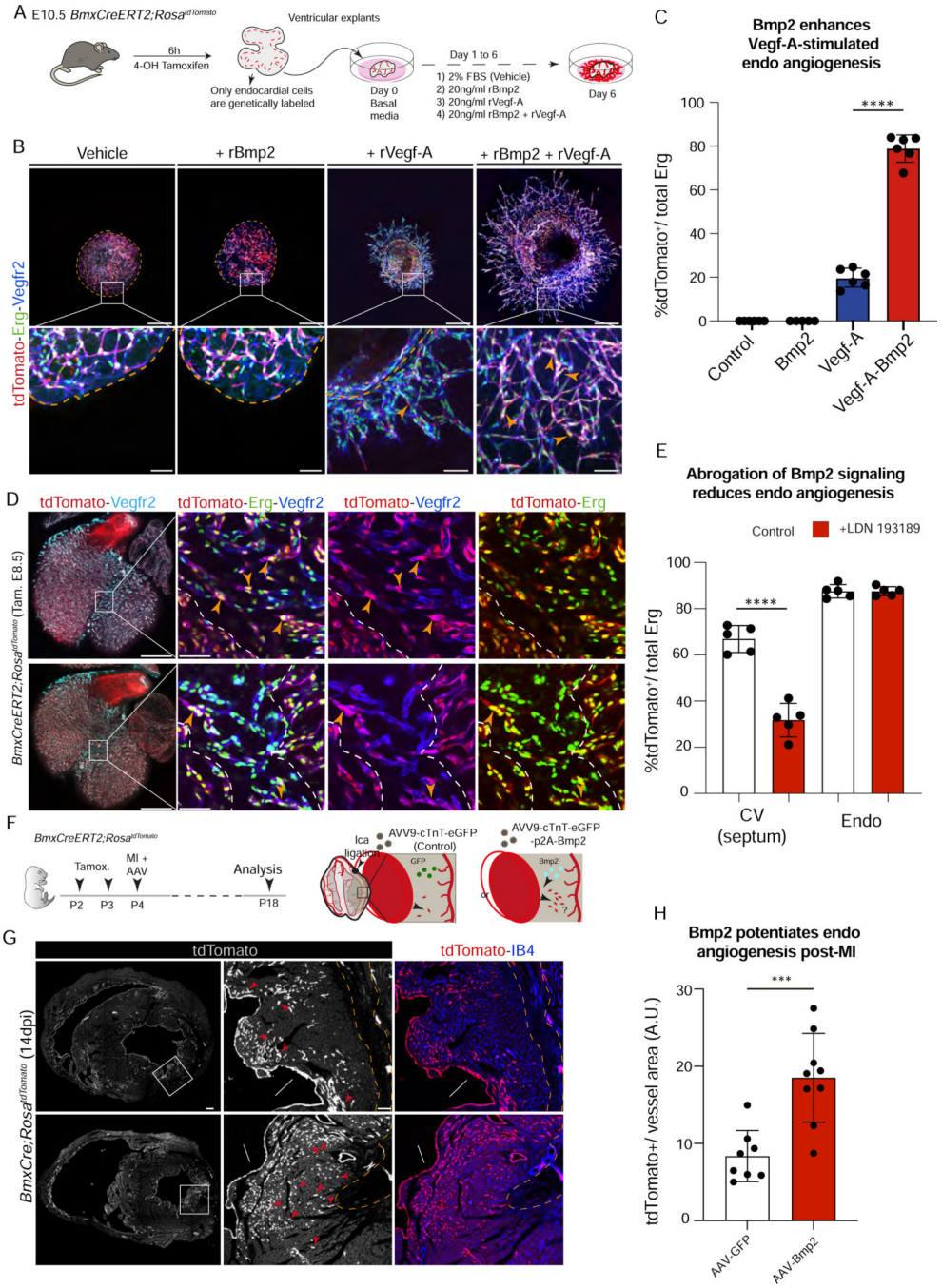

Figure 6. Bmp2 potentiates endo-derived CV angiogenesis in culture and neonatal hearts.

A) Experimental strategy for **B** and **C**. **B** and **C)** Immunostaining **(B)** and quantification **(C)** showed combining Vegfa and Bmp2 stimulates endo-derived CVs sprouting (arrowheads). (rBmp2, $n = 5$ explants; Vegfa, $n = 6$ explants; combination, $n = 6$ explants) **D)** Whole-mount ventral view of heart treated with Bmp signaling inhibitor (+ LDN 193189) or PBS (control). Magnifications highlight septal region where endo-derived CV ECs are sprouting. Dotted lines demarcate endocardium (endo) from endo-derived CV ECs within septum. **E)** Quantification of experiment in D showing the total number of lineage-labeled cells

in the ventral septum and endo compartments (n = 4 Control; n =5 +LDN 193185). **F)** Experimental strategy for **G** and **H**. **G)** P18 tissue sections from lineage-labeled and injured hearts. Boxed regions show increased endo-derived CVs (arrowheads) in the left ventricles injected with AAV expressing Bmp2 injected hearts (n = 9 hearts, lower panels) compared with vehicle-treated hearts (n=8, upper panels). **H)** Quantification of experiment in **G**. Scale bar=200 pM in B, D and E (full view). Scale bar=50 pM in B, D and E (boxed regions). Data are mean ± s.d. ***P ≤ 0.001, ****, P ≤ 0.0001, by Student's t-test.

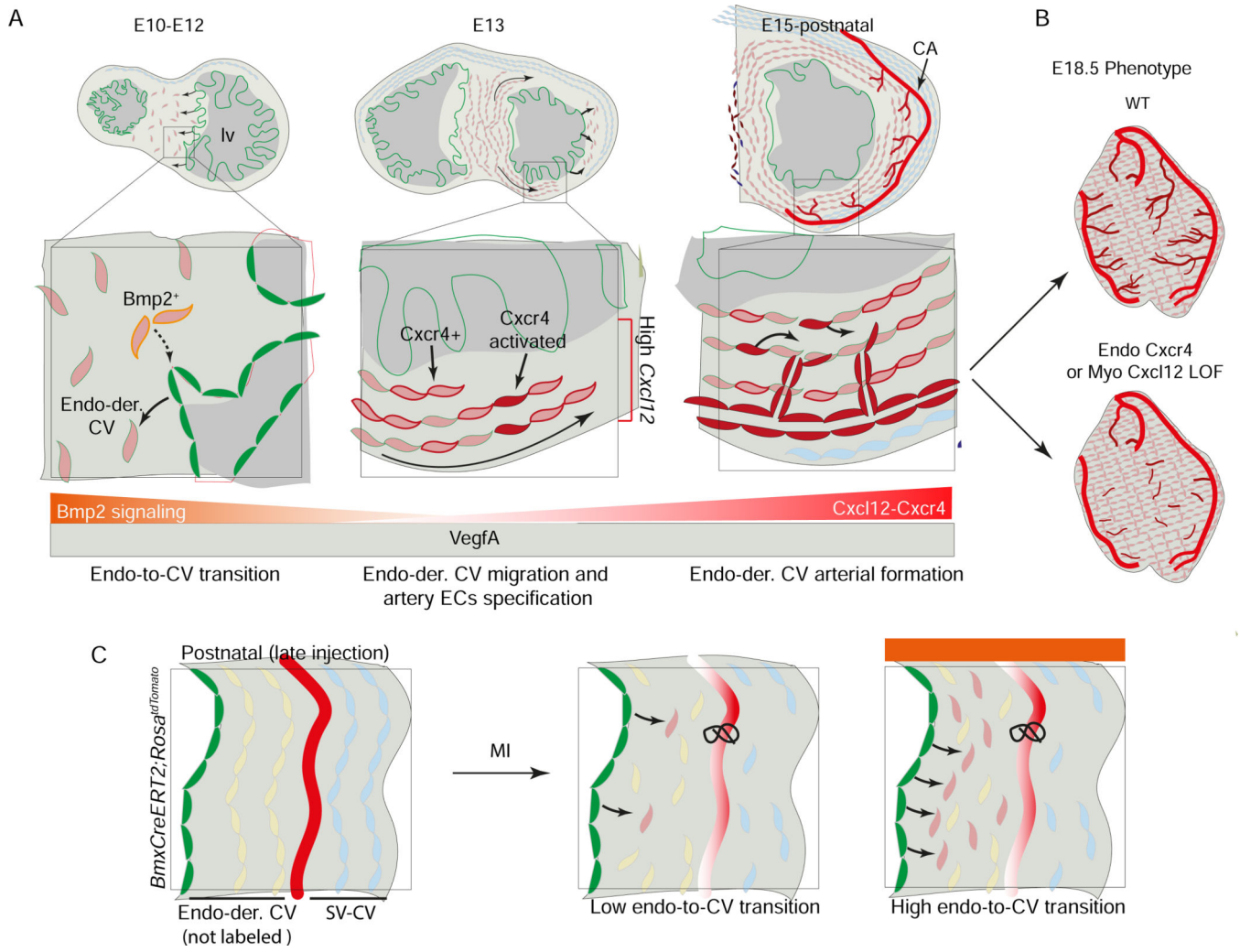

Figure 7. Model for sequential Bmp2-Cxcr4 signaling driving endo-to-CV ECs transition and artery formation during heart development and regeneration.

A) Endo cells (green) differentiate into CV ECs (light red) within the developing septum. CV ECs expressing *Bmp2* signal to adjacent endo (dotted arrow) to favor endo-to-CV ECs transition. As development precedes, septal endo-derived CV ECs migrate ventrally into myocardial free wall. Cardiomyocytes expressing *Cxcl8* guide a subset of Cxcr4+ endo-derived CV ECs (red) o form arteries. **B)** Early deletion of *Cxcr4* in endo or deletion of myocardial *Cxcl12* disrupts endo-derived artery formation in the ventral side of the heart. **C)** Exogenous administration of Bmp2 greatly enhances endo-to-CV ECs transition in subendocardial space in neonatal mice subjected to experimental MI.

Key resources table

REAGENT or RESOURCE	SOURCE	IDENTIFIER
Antibodies		
Anti-VEGFR2	R&D Systems	Cat. # AF644
Anti-CX40	Alpha Diagnostics Int.	Cat. # CX40-A
Anti-ERG	Abcam	Cat. # ab92513; RRID: AB_2630401
Anti-ENDOMUCIN	Invitrogen	Cat. # 14-5851-82
Anti-CDH5	BD Pharmingen	Cat. # 550548; RRID: AB_2244723
Anti-CXCR4	Abcam	Cat. # ab124824; RRID: AB_10975635
Anti-Jaggedl	R&D Systems	Cat. # AF1277
Anti-CD31	BD Pharmingen	Cat. # 557355; RRID: AB_396660
Anti-TnnI3	Abcam	Cat. # ab47003; RRID: AB_47002
Anti-ESR (prediluted)	Abcam	Cat. # ab27595
Anti-RFP	Rockland	Cat. # 600-401-379
Isolectin GS-IB4 Alexa Fluor™ 647 Conjugate	Invitrogen	Cat. # I32450
Alexa fluor-conjugated antibodies (405, 488, 555, 633)	Life Technologies	N/A
Anti-Digoxigenin-AP, Fab fragments	Roche diagnostics	Cat.: # 11093274910
Anti-Digoxigenin-POD, Fab fragments	Roche diagnostics	Cat.: # 11207733910
Rat Anti- APC/Cy7 Cd45 (rat monoclonal)	Biolegend	Cat.: # 103116; RRID: AB_312981
Rat anti- APC Pecaml (rat monoclonal)	Biolegend	Cat.: # 102410; RRID: AB_312905
Rat anti- APC-Cy7 Ter119 (rat monoclonal)	Biolegend	Cat.: # 116223; RRID: AB_2137788
Bacterial and virus strains		
DH5-alpha Competent E. coli (High Efficiency)	New England Biolabs	Cat.: # C2987H
NEB® Stable Competent E. coli	New England Biolabs	Cat.: # C3040H
Biological samples		
Chemicals, peptides, and recombinant proteins		
PFA	Electron Microscopy Sciences	Cat.: # 15714
Proteinase K	Millipore Sigma	Cat. #3115879001
Acetic anhydride	Millipore Sigma	Cat. # SHBC1816V
Formamide	Millipore Sigma	Cat. # F 9037
Saline Sodium Citrate (SSC, 20x)	Millipore Sigma	Cat. # 93017-10L-F
Danhardt's solution	Millipore Sigma	Cat. # D 2532
CHAPS	Millipore Sigma	Cat. # C5070
Yeast RNA	Millipore Sigma	Cat. # R 6750
Triethanolamine	Millipore Sigma	Cat. # BCBK5944V
Hydrogen peroxide 30%	Millipore Sigma	Cat. # 7722-84-1
BM-Purple	Roche Diagnostic	Cat. #1144207400
Donkey Serum	Jacksonimmuno	Cat #: 017-000-121; RRID: AB_2337258
rBMP2	R&D Systems	Cat. # 355-BM-010/CF

REAGENT or RESOURCE	SOURCE	IDENTIFIER
rVEGFA-165	PeproTech	Cat. # 450-32
LDN-193189	Millipore Sigma	Cat. # SML0559-5MG
Fetal Bovine Serum	Millipore Sigma	Cat. # F2442
Matrigel	Corning	Cat.: # 354230
Tamoxifen	Millipore Sigma	Cat.: # T5648
4-OH Tamoxifen	Millipore Sigma	Cat.: # H6278
Collagenase IV	Worthington	Cat.: # LS004186
Dispase	Worthington	Cat #: LS02100
DNase I	Worthington	Cat #: LS002007
Critical commercial assays		
Roche DIG RNA Labeling kit	Roche Diagnostic	Cat.: # 11175025910
RNEasy Mini Kit	Qiagen	Cat.: # 74,104
AAVpro® Purification Kit Maxi (All Serotypes)	Takara	Cat.: # 6675
ZymoPURE II Plasmid Maxiprep Kit	Zymo Research	Cat.: # D4203
Deposited data		
scRNA-seq on E127.5 BmxCreERT2 ;RosatdT omato : Cxcr4flox	This paper	GEO: GSE2149942
scRNA-seq on E12 BmxCreERT2;RosatdTomato	scRNA-seq generated by Phansalkar et al.[29]	https://doi.org/10.5061/dryad.h70rxwdjh
scRNA-seq on E17.5 BmxCreERT2;RosatdTomato	scRNA-seq generated by Phansalkar et al.[29]	https://doi.org/10.5061/dryad.h70rxwdjh
Experimental models: Organisms/strains		
CD1	Charles River Laboratories	Strain Code:# 022
Cxcl12 fl/fl	The Jackson Laboratory	Stock:# 021773
Cxcr4 fl/fl	The Jackson Laboratory	Stock:# 008767
Cxcl12-DsRed	The Jackson Laboratory	Stock:# 022458
Rosa26-TdTomato	The Jackson Laboratory	Stock:# 007909
Rosa26-nTdTomato	The Jackson Laboratory	Stock:# 025106
pTRE-H2BGFP	The Jackson Laboratory	Stock:# 005104
BmxCreERT2	Mouse line generated by Ehling et al.[22]	N/A
Cxcr4Tango	This paper	N/A
Recombinant DNA		
pENN.AAV.cTNT.PI.eGFP.WPRE	Addgene	Cat.: # 105543
pAdDeltaF6	Addgene	Cat.: #112867
pAAV2/9	Addgene	Cat.: #112865
pBSK(−)mNpr3	This paper	
pBSK(−)mCldn5	This paper	
Software and algorithms		
Seurat v4	Hao et al.[39]	https://satijalab.org/seurat/
scCustomise	scCustomise	https://samuel-marsh.github.io/scCustomize/

REAGENT or RESOURCE	SOURCE	IDENTIFIER
CellChat	Jin et al.[40]	https://github.com/sqjin/CellChat
asc-seurat	Pereira et al.[41]	https://github.com/KirstLab/asc_seurat/blob/main/docs/trajectoryinference.rst
CytoTRACE	Gulati et al.[37]	https://cytotrace.stanford.edu/
FIJI	NIH	https://imagej.net/software/fiji/
Prism 9	GraphPad Software	http://www.graphpad.com/scientific-software/prism/
Other		
DAPI (4',6-diamidino-2-phenylindole)	Millipore Sigma	Cat.: # D9542-1MG
8.0 uM PET membrane culture inserts	Millipore Sigma	MCEP24H48
Fluoromount G (Southerm Biotech; Cat: 0100-01)	(Southerm Biotech	Cat.: #0100-01